

Mechanical studies on the formation and destruction of carbon monoxide (CO), carbon dioxide (CO₂), and carbon trioxide (CO₃) in interstellar ice analog samples†

Chris J. Bennett,^{ab} Corey S. Jamieson^a and Ralf I. Kaiser^{*ab}

Received 19th August 2009, Accepted 5th February 2010

First published as an Advance Article on the web 1st March 2010

DOI: 10.1039/b917162b

A series of ice mixtures containing carbon monoxide (CO), carbon dioxide (CO₂), and molecular oxygen (O₂) with varying carbon-to-oxygen ratios from 1 : 1.5 to 1 : 4 were irradiated at 10 K with energetic electrons to derive formation mechanisms and destruction pathways of carbon monoxide (CO), carbon dioxide (CO₂), and carbon trioxide (CO₃) in extraterrestrial, low temperature ices. Reactants and products were analyzed on line and *in situ* via absorption–reflection–absorption FTIR spectroscopy in the solid state, while the gas phase was sampled by a quadrupole mass spectrometer (QMS). Additionally, isotopically mixed ices consisting of (i) ¹³CO : C¹⁸O : CO₂, (ii) CO₂ : C¹⁸O₂, and (iii) CO₂ : ¹⁸O₂ were irradiated in order to derive mechanical and kinetic information on the production and destruction pathways of the following species: (i) ¹³CO, C¹⁸O, CO₂, CO, ¹³CO₂, ¹⁸OCO, and ¹³CO₃ (C_{2v}), (ii) CO₂, C¹⁸O₂, CO, C¹⁸O, ¹⁸OCO, CO₃ (C_{2v}), OC¹⁸OO (C_{2v}), OC¹⁸O₂ (C_{2v}), ¹⁸OCO₂ (C_{2v}), ¹⁸OC¹⁸OO (C_{2v}), and C¹⁸O₃ (C_{2v}), and (iii) CO₂, CO, ¹⁸OCO, C¹⁸O, and C¹⁸O₂.

1. Introduction

Ices containing carbon monoxide (CO) and carbon dioxide (CO₂) have been identified within a wide range of solar system bodies and also constituents of interstellar grains. According to a recent survey of 23 infrared sources using the *Infrared Space Observatory* (ISO), their abundances relative to water within interstellar ices were found to range from 3% to 25% for carbon monoxide and from 8% to 35% for carbon dioxide.¹ The high abundances of these molecules relative to water are also present in solar system observations of icy bodies. Measurements of Oort cloud comets indicate that the abundance of carbon monoxide may be up to 17% relative to water,² whereas the fraction of carbon dioxide is typically about 6%.³ Considering the icy satellites of the Jovian system, carbon dioxide ice has been detected on Europa, Callisto and Ganymede.^{4,5} Within the Saturnian system, carbon dioxide ice has also been probed on Enceladus, Dione, Hyperion, Iapetus, and Phoebe.^{6–8} Considering the Uranian Satellites, carbon dioxide ice has been monitored on the surfaces of Ariel, Umbriel, and Titania.^{9,10} Triton, Neptune's largest moon, has ices of not only containing carbon dioxide but also carbon monoxide.¹¹ Ices of carbon monoxide have also been positively identified on the dwarf planet Pluto.¹²

These ices are subject to radiation from both the solar wind and Galactic Cosmic Radiation (GCR); the flux of the solar

wind decreases with a $1/r^2$ dependence, r being the distance from the sun, and thus becomes less important when the outer solar system is considered. According to ref. 13, the solar radiation consists of solar photons ($\phi \approx 2.6 \times 10^{15} \text{ cm}^{-2} \text{ s}^{-1}$ at 1 AU; $E > 3.9 \text{ eV}$), ions ($\phi \approx 4 \times 10^8 \text{ cm}^{-2} \text{ s}^{-1}$ at 1 AU; about 96% H⁺ and 4% He²⁺, few heavier nuclei at 1 keV amu⁻¹), and electrons ($\phi \approx 4 \times 10^8 \text{ cm}^{-2} \text{ s}^{-1}$ at 1 AU; $E \approx 12 \text{ eV}$). The flux of the GCR on the other hand is considered nearly isotropic throughout the galaxy and consists of around 98% H⁺, 2% He²⁺, and few heavier nuclei; the energy distribution maximum peaks at around 10 MeV where a fluence of around $\phi = 10 \text{ cm}^{-2} \text{ s}^{-1}$ is found.¹⁴ Large planetary bodies may also have substantial magnetospheres associated with them which also contain significant sources of keV energy ions and electrons (*e.g.* ref. 15).

In order to correlate the observed chemical abundances of the carbon oxides, it is important to understand the evolution of astrophysically relevant ices as they are chemically processed *via* their surrounding radiation environments. Here, the main focus of this investigation is to study the irradiation effects on the production and destruction of carbon monoxide, carbon dioxide, and carbon trioxide within these environments. When pure carbon monoxide ices are irradiated, no oxygen rich species were produced except carbon dioxide (ref. 16). The other molecules identified are linear cumulenic chains such as carbon chains (C₃ and C₆) together with oxygen-terminated carbon clusters of the series C_{*n*}O ($n = 2–7$) and C_{*n*}O₂ ($n = 3–5$, and 7). In contrast, when pure carbon dioxide is irradiated, it initially decomposes into carbon monoxide and suprathreshold oxygen atoms. The oxygen atoms are incorporated into cyclic ring structures, *i.e.* higher carbon oxides, of the form O=C(O_{*n*}), where species with $n = 2–5$ have previously been identified.^{17–20} Considering the case of

^a Department of Chemistry, University of Hawaii at Manoa, Honolulu, HI 96822, USA

^b Institute for Astronomy and NASA Astrobiology Institute, 2680 Woodlawn Drive, University of Hawaii, Honolulu, HI 96822, USA. E-mail: ralfk@hawaii.edu

† Electronic supplementary information (ESI) available: Color versions of the individual spectra found in Fig. 1, as well as a color version of Fig. 5. See DOI: 10.1039/b917162b

carbon trioxide, CO₃, the C_{2v} isomer is energetically more stable; however, the D_{3h} isomer of carbon trioxide has also been identified as a product of irradiated carbon dioxide ices.²¹ Although carbon trioxide has yet to be detected in an extra-terrestrial environment, it is a major product generated when carbon dioxide ices are irradiated; therefore it is not surprising that this molecule has been proposed as a candidate molecule to be searched for on the Galilean icy satellites,²² and is also a feasible component of interstellar ices—for this reason we shall also discuss its likely formation mechanisms. Here, as part of a systematic study, we have selected three different ice compositions containing varying carbon-to-oxygen (C : O) ratios of 1 : 1.5, (CO : CO₂) 1 : 2 (CO₂), and 1 : 4 (CO₂ : O₂) and exposed them to radiation using energetic electrons. Here, we note that these three molecular species (CO, CO₂, and O₂) represent three out of four key components of apolar interstellar ices (the fourth being molecular nitrogen, N₂) and thus this investigation is particularly relevant to this astronomical environment.²³ The benefits of utilizing this specific radiation source is that it effectively simulates energetic electrons formed in the track of cosmic ray particles within ices as discussed elsewhere.²⁴ In addition, isotopic labeling has been used in order to obtain mechanistical information and to ‘trace’ the fate of carbon (¹³C) and oxygen (¹⁸O) atoms within complex ice mixtures effectively.

2. Experimental

The details of our experimental set up as well as the quantification of the column densities and ice thicknesses can be found elsewhere.¹⁷ Briefly, the experiments are conducted in an ultrahigh vacuum (UHV) chamber, where oil-free magnetically suspended turbomolecular pumps are used to bring the base pressure down to around 5×10^{-11} Torr. The gases are condensed at 10 K onto a freely rotatable highly polished silver monocrystal (area = 3.0 ± 0.4 cm²) situated in the center of the chamber. This condensed phase is sampled by a Nicolet 6700 Fourier Transform Infrared (FTIR) spectrometer operating in absorption–reflection–absorption mode at a reflection angle of 75° (spectra are recorded in succession over the range 5000–400 cm⁻¹ at a resolution of 4 cm⁻¹, each integrated over up to 2.5 min) on-line and *in situ*. Gaseous

species are analyzed by a quadrupole mass spectrometer (Balzer QMG 420) using 100 eV electron impact ionization, operated at 90° off-axis running as a residual gas analyzer. Use of a secondary electron multiplier enables sensitivity around 150 A Torr⁻¹. During each experiment, a gas mixture is produced and condensed on the silver target through a glass capillary array whereby the base condensation pressure ($2\text{--}10 \times 10^{-8}$ Torr) and deposition time of up to 7 min are controlled to ensure reproducible thicknesses. Ices were irradiated with 5 keV electrons for one hour; typically, the samples were then left isothermally for up to 60 min before being warmed to 300 K at a rate of 0.5 K min⁻¹. Table 1 compiles the experimental conditions throughout this investigation.

In the case of CO : CO₂ ices, the CO column density was derived from the area of the ¹³CO fundamental band, using an absorption coefficient of 1.1×10^{-17} cm molecule⁻¹²⁵ and then multiplying by 100/1.1 to account for the abundance of the ¹³CO present. For carbon dioxide, the area of the 2ν₂ + ν₃ combination band at 3600 cm⁻¹ was utilized to estimate the column density taking the absorption coefficient as 4.5×10^{-19} cm molecule⁻¹.²⁵ Here, we find column densities of $6.2 \pm 0.1 \times 10^{17}$ molecules cm⁻² for CO, and $9.8 \pm 0.2 \times 10^{17}$ molecules cm⁻² for CO₂ giving a ratio in the ice of 0.6 : 1 (CO : CO₂). For the ¹³CO : C¹⁸O : CO₂ ice, the area of the 2ν₂ + ν₃ combination band at 3599 cm⁻¹ was used to derive the column density for carbon dioxide as $6.1 \pm 0.3 \times 10^{17}$ molecules cm⁻². The areas of the fundamental bands ¹³CO and C¹⁸O bands, identified at 2095 and 2087 cm⁻¹, were used to derive the column densities of $9.1 \pm 0.2 \times 10^{16}$ molecules cm⁻² and $8.9 \pm 0.2 \times 10^{16}$ molecules cm⁻², for the respective isotopomers. Thus, the actual ratios within the ice are given as 1 : 1 : 7 (¹³CO : C¹⁸O : CO₂). Secondly, considering the CO₂ : C¹⁸O₂ ice, an averaged value was taken from the areas of the 2ν₂ + ν₃ combination band (at 3604 and 3519 cm⁻¹, respectively), the ν₁ + ν₃ combination band (at 3713 and 3628 cm⁻¹, respectively), and the corresponding ¹³C isotopomers of the ν₃ fundamentals (at 2281 and 2246 cm⁻¹, respectively, multiplied by 100/1.1). The absorption coefficients for ν₃ and ν₁ + ν₃ were taken as 7.6×10^{-17} cm molecule⁻¹ and 1.4×10^{-18} cm molecule⁻¹, respectively.²⁵ The derived column densities were thus $2.3 \pm 0.6 \times 10^{17}$ molecules cm⁻² for CO₂, and $2.5 \pm 2.1 \times 10^{17}$ molecules cm⁻² for C¹⁸O₂. Here, additional

Table 1 Experimental parameters used within this study (see text for additional details)

Ice mixture	Initial gas mixture/ mbar	Column density in ice/ molecules cm ⁻²	Irradiation current/ μA	Irradiation time/ min	Electron flux ^b / cm ⁻² s ⁻¹
CO : CO ₂	154 (CO)	$6.15 \pm 0.12 \times 10^{17}$ (CO)	0.1	60	1.6×10^{11}
	141 (CO ₂)	$9.78 \pm 0.23 \times 10^{17}$ (CO ₂)			
¹³ CO : C ¹⁸ O : CO ₂	26 (¹³ CO)	$9.09 \pm 0.21 \times 10^{16}$ (¹³ CO)	0.1	60	1.6×10^{11}
	25 (C ¹⁸ O)	$8.93 \pm 0.19 \times 10^{16}$ (C ¹⁸ O)			
	35 (CO ₂)	$6.05 \pm 0.30 \times 10^{17}$ (CO ₂)			
CO ₂ : C ¹⁸ O ₂	19 (CO ₂)	$2.30 \pm 0.60 \times 10^{17}$ (CO ₂)	0.1	60	1.6×10^{11}
	19 (C ¹⁸ O ₂)	$2.46 \pm 0.14 \times 10^{17}$ (C ¹⁸ O ₂)			
CO ₂ : O ₂	20 (CO ₂)	$9.37 \pm 0.47 \times 10^{16}$ (CO ₂)	1	180	1.6×10^{12}
	80 (O ₂)	$1.08 \pm 0.08 \times 10^{18}$ ^a (O ₂)	5	60	8.2×10^{12}
CO ₂ : ¹⁸ O ₂	21 (CO ₂)	$9.24 \pm 0.46 \times 10^{16}$ (CO ₂)	1	180	1.6×10^{12}
	79 (¹⁸ O ₂)	$1.07 \pm 0.08 \times 10^{18}$ ^a (¹⁸ O ₂)	5	60	8.2×10^{12}

^a Ratio was quantified with the mass spectrometer through matrix interval algebra. ^b Calculated using an extraction efficiency of 78.8%, as stated by the manufacturer for the electron source.

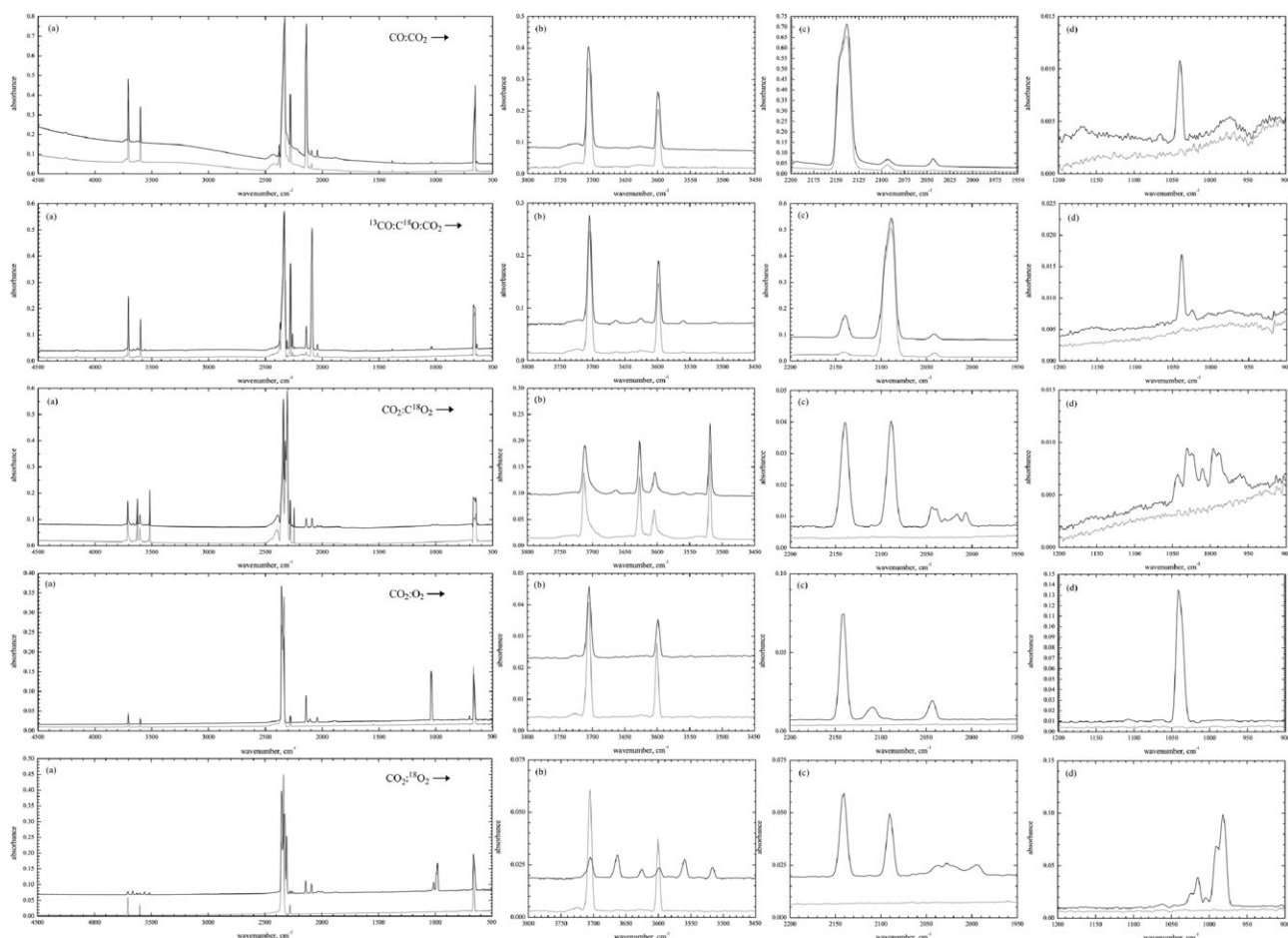


Fig. 1 Infrared spectra of ice mixtures prior to (gray line) and after the irradiation (black line) shown over several different wavelength ranges: (a) 500–4500 cm^{-1} , (b) 3450–3800 cm^{-1} , (c) 1950–2200 cm^{-1} , (d) 1800–1950 cm^{-1} . The absorption axis has been shifted for clarity. Note that each row corresponds to a different ice composition as denoted by the arrow. Please see the ESI† for color versions of each of the individual spectra.

bands were required to determine the thickness more accurately, due to an unexpected change in the relative intensities of the two combination bands, as is reflected from the large error bars derived (see Fig. 1b). Finally, in the case of the $\text{CO}_2 : \text{O}_2$ ice, the area of the $2\nu_2 + \nu_3$ combination band at 3600 cm^{-1} was used to derive a column density for carbon dioxide of $9.4 \pm 0.5 \times 10^{16} \text{ molecules cm}^{-2}$. As molecular oxygen is infrared inactive, the signals from the mass spectrometer during warm-up of a blank (non-irradiated) sample were recorded and integrated. By use of matrix interval algebra²⁶ we were able to determine the ratio to be 1 : 12 ($\text{CO}_2 : \text{O}_2$), which was consistent with the $\text{CO}_2 : ^{18}\text{O}_2$ ice samples which were prepared in an identical manner. For the $\text{CO}_2 : ^{18}\text{O}_2$ ice, the area of the $\nu_1 + \nu_3$ combination band at 3705 cm^{-1} was used to derive a column density of $9.2 \pm 0.5 \times 10^{16} \text{ molecules cm}^{-2}$ for carbon dioxide.

3. Results

The results have been organized in a manner so that comparisons can easily be made between each experiment. For each of the ices investigated, we shall focus sequentially on the findings relating to carbon monoxide, carbon dioxide, and carbon trioxide; a brief discussion of other species identified is

also presented. The infrared spectra of each ice prior (gray lines) and after (black lines) the irradiation are compiled in Fig. 1, and enlarged color versions of each figure can be found within the ESI;† the corresponding vibrational assignments are given in Table 2. Please note that a deviation of a few cm^{-1} between experiments or literature values is expected due to the differing chemical environments. As the samples were heated, the mass spectrometer sampled molecules sublimated into the gas phase; Table 3 shows the peak values of the ion intensities during sublimation events, which were recorded for the relevant isotopomers of carbon monoxide, carbon dioxide, molecular oxygen, and ozone.

3.1 CO : CO₂ experiments

3.1.1 Carbon monoxide. The carbon monoxide fundamental is identified at 2139 cm^{-1} (Fig. 1c) and has a shoulder band found at 2146 cm^{-1} ; this is in accordance with previous studies where the same features are identified at 2139 and 2143 cm^{-1} , respectively.²⁷ The $2\nu_1$ overtone band was found at 4256 cm^{-1} in agreement with ref. 28 who reported a position of 4254 cm^{-1} . The ^{13}CO isotopomer of carbon monoxide absorbed at 2093 cm^{-1} , compared to 2092 cm^{-1} as determined previously.²⁸ The area of the fundamental band was found to increase upon irradiation. During the warm-up period, the

Table 2 Species identified in the infrared spectra of ice mixtures before (marked with an asterisk) and after irradiation of the ices energetic electrons

Assignment	Peak positions				
	CO : CO ₂	¹³ CO : C ¹⁸ O : CO ₂	CO ₂ : C ¹⁸ O ₂	CO ₂ : O ₂	CO ₂ : ¹⁸ O ₂
CO					
ν_1	2146*, 2139* 2093* (¹³ CO)	2140* 2095* (¹³ CO) 2087* (C ¹⁸ O) 2041* ^c (¹³ C ¹⁸ O)	2140 2089 (C ¹⁸ O)	2142	2141 2090 (C ¹⁸ O)
$2\nu_1$	4256*	4162* (¹³ CO) 4156* (C ¹⁸ O)	—	4257	—
CO ₂					
ν_1	1276*	1276*	1277* 1340* (C ¹⁸ O ₂)	—	1279*
ν_2	667*, 665* 640* (¹³ CO ₂)	667*, 657* 642*, 639* (¹³ CO ₂)	668*, 658* 652*, 646* (C ¹⁸ O ₂) 638* (¹³ CO ₂) 629* (¹³ C ¹⁸ O ₂)	667*, 658*	668*, 660* br ^a
ν_3	2354* 2331* (¹⁸ OCO) 2280* (¹³ CO ₂)	2334 (CO ₂) 2327* (¹⁸ OCO) 2309* (C ¹⁸ O ₂) 2279* (¹³ CO ₂) 2262 (¹⁸ O ¹³ CO) 2243* (¹³ C ¹⁸ O ₂)	2341* 2328* (¹⁸ OCO) 2307* (C ¹⁸ O ₂) 2281* (¹³ CO ₂) 2264* (¹⁸ O ¹³ CO) 2246* (¹³ C ¹⁸ O ₂)	2357*, 2337* 2326* (¹⁸ OCO) 2280* (¹³ CO ₂)	2359*, 2336* 2327* (¹⁸ OCO) 2310 (C ¹⁸ O ₂) 2280* (¹³ CO ₂) 2262 (¹⁸ O ¹³ CO) 2244 (¹³ C ¹⁸ O ₂)
$2\nu_2$	1384*	1383*	1384* 1228* (C ¹⁸ O ₂)	1382*	1383*
$\nu_1 + \nu_3$	3700*	3705* 3664* (¹⁸ OCO) 3626* (¹³ CO ₂)	3713* 3663 (¹⁸ OCO) 3628* (C ¹⁸ O ₂)	3705*	3705* 3663 (¹⁸ OCO) 3626 (C ¹⁸ O ₂)
$2\nu_2 + \nu_3$	3600*	3599* 3560* (¹⁸ OCO) 3513* (¹³ CO ₂)	3604* 3560 (¹⁸ OCO) 3519* (C ¹⁸ O ₂)	3600*	3601* 3560 (¹⁸ OCO) 3517* (C ¹⁸ O ₂)
O ₂					
ν_1	1613 ^b	1612 ^b		1550* 1610 ^b	1508 (¹⁸ OO) 1463* (¹⁸ O ₂)
O ₃					
ν_1			—	1107	1038 ^c (¹⁸ O ₃)
ν_2			—	705	
ν_3	1040	1038 1025 (¹⁸ OO ₂) 1003 (O ¹⁸ OO)	1043 1031 (¹⁸ OO ₂) 1023 (¹⁸ OO ¹⁸ O) 1010 (O ¹⁸ OO) 996 (O ¹⁸ O ₂) 989 (¹⁸ O ₃)	1041	1038 ^c 1024 (¹⁸ OO ₂) 1015 (¹⁸ OO ¹⁸ O) 1004 (O ¹⁸ OO) 991 (O ¹⁸ O ₂) 981 (¹⁸ O ₃)
$\nu_1 + \nu_3$			—	2109	br 1995 (¹⁸ O ₃)
CO ₃ (C _{2v})					
ν_1	2042	2041* ^c 1988 (¹³ CO ₃)	2045 2039 (OC ¹⁸ OO) 2031 (OC ¹⁸ O ₂) 2025 (¹⁸ OCO ₂) 2018 (¹⁸ OC ¹⁸ OO) 2008 (¹⁸ OC ¹⁸ O ₂)	2044	br
ν_2	1065	1066	br	—	br
ν_5	973	—	—	—	—
fermi	1890	br	br	1896	br
CO ₃ (D _{3h})					
ν_1/ν_2	1168	br	br	1167	br

^a br—broad features in this region make it difficult to assign distinct isotopomers of the carriers. ^b These features have been observed during irradiation of pure molecular oxygen, and appear to be associated with this molecule. ^c Due to the fact that these features overlap, they could not be uniquely distinguished.

mass spectrometer signal corresponding to CO ($m/z = 28$) was found to mostly sublimate around 49–53 K, delayed from values in pure carbon monoxide ices where it is found to sublime closer to 37 K.¹⁶ A second sublimation event occurs as the carbon dioxide sublimates resulting from trapped CO species; however, fragmentation of the CO₂ molecule will also contribute to the observed signal.

3.1.2. Carbon dioxide. The most intense band of carbon dioxide is associated with the asymmetric stretching fundamental (ν_3) which was observed at 2354 cm⁻¹ in good agreement with previous studies.^{29,30} The ν_2 bending mode is probed at 665 and 667 cm⁻¹.^{29,30} The ν_1 symmetric stretch and $2\nu_2$ overtone weakly interact giving a Fermi doublet which is detectable at 1276 and 1384 cm⁻¹.³¹ Also clearly observable

Table 3 The observed peak current intensities (in units of Amperes) observed with the mass spectrometer at given temperatures (in Kelvin) during the warming up of the irradiated ice mixtures for CO₂, O₂, and O₃ with comparative signals from isotopomers of these species where they were detected. The results are presented in order of decreasing C : O ratio present within the initial ice mixture

Peak ion current recorded/A						
C : O ratio	Ice mixture	Temperature/K	CO	CO ₂	O ₂	O ₃
1 : 1.5	CO : CO ₂	34	—	—	1.2 × 10 ⁻⁹	—
		49–53	3.8 × 10 ⁻⁷	—	1.9 × 10 ⁻⁹	—
		70	—	—	5.4 × 10 ⁻¹⁰	2.6 × 10 ⁻¹¹
		91–92	1.4 × 10 ⁻⁷	5.2 × 10 ⁻⁷	6.8 × 10 ⁻¹⁰	2.0 × 10 ⁻¹¹
		30	2.5 × 10 ⁻⁸	—	8.4 × 10 ⁻¹⁰	—
1 : 1.5	¹³ CO : C ¹⁸ O : CO ₂	45	8.4 × 10 ⁻⁸	1.3 × 10 ⁻¹⁰ (¹³ CO ₂)	1.5 × 10 ⁻⁸	—
			7.9 × 10 ⁻⁸ (¹³ CO)	1.2 × 10 ⁻¹⁰ (¹⁸ OCO)	8.0 × 10 ⁻¹¹ (¹⁸ OO)	—
			7.3 × 10 ⁻⁸ (C ¹⁸ O)	—	3.6 × 10 ⁻¹³ (¹⁸ O ₂)	—
			1.6 × 10 ⁻⁹ (¹³ C ¹⁸ O)	—	—	—
		47–49	1.0 × 10 ⁻⁷	1.3 × 10 ⁻¹⁰ (¹³ CO ₂)	1.7 × 10 ⁻⁸	—
			1.4 × 10 ⁻⁷ (¹³ CO)	1.2 × 10 ⁻¹⁰ (¹⁸ OCO)	1.5 × 10 ⁻¹⁰ (¹⁸ OO)	—
			1.2 × 10 ⁻⁷ (C ¹⁸ O)	—	1.0 × 10 ⁻¹² (¹⁸ O ₂)	—
			2.7 × 10 ⁻⁹ (¹³ C ¹⁸ O)	—	—	—
		67–68	—	—	2.9 × 10 ⁻¹⁰	3.9 × 10 ⁻¹¹
			—	—	4.6 × 10 ⁻¹¹ (¹⁸ OO)	1.2 × 10 ⁻¹² (¹⁸ OO ₂ /O ¹⁸ OO)
1 : 2	CO ₂ : C ¹⁸ O ₂	91–92	1.8 × 10 ⁻⁸	2.8 × 10 ⁻⁷	2.7 × 10 ⁻¹⁰	—
			1.6 × 10 ⁻⁹ (¹³ CO)	5.9 × 10 ⁻⁹ (¹³ CO ₂)	6.4 × 10 ⁻¹² (¹⁸ OO)	—
			1.4 × 10 ⁻⁹ (C ¹⁸ O)	4.9 × 10 ⁻⁹ (¹⁸ OCO)	—	—
			3.7 × 10 ⁻¹¹ (¹³ C ¹⁸ O)	3.6 × 10 ⁻¹⁰ (¹⁸ O ¹³ CO)	—	—
			—	2.8 × 10 ⁻¹⁰ (C ¹⁸ O ₂)	—	—
			—	4.9 × 10 ⁻¹¹ (¹³ C ¹⁸ O ₂)	—	—
		40	—	—	8 × 10 ⁻¹¹	—
			—	—	1.2 × 10 ⁻¹⁰ (¹⁸ OO)	—
			—	—	6 × 10 ⁻¹¹ (¹⁸ O ₂)	—
			—	—	—	—
1 : 4	CO ₂ : O ₂	47	1.4 × 10 ⁻⁹	—	7.0 × 10 ⁻¹⁰	3.0 × 10 ⁻¹¹ (¹⁸ OO ₂ /O ¹⁸ OO)
			1.3 × 10 ⁻⁹ (C ¹⁸ O)	—	1.2 × 10 ⁻⁹ (¹⁸ OO)	3.5 × 10 ⁻¹¹ (O ¹⁸ O ₂ / ¹⁸ OO ¹⁸ O)
		64–72	4.5 × 10 ⁻⁹	—	6.2 × 10 ⁻¹⁰ (¹⁸ O ₂)	3.0 × 10 ⁻¹² (¹⁸ O ₃)
			4.2 × 10 ⁻⁹ (C ¹⁸ O)	—	3.8 × 10 ⁻¹⁰	2.8 × 10 ⁻¹¹ (¹⁸ OO ₂ /O ¹⁸ OO)
		91	3.0 × 10 ⁻⁸	3.1 × 10 ⁻⁷	6.3 × 10 ⁻¹⁰ (¹⁸ OO)	2.7 × 10 ⁻¹¹ (O ¹⁸ O ₂ /O ¹⁸ OO)
			2.8 × 10 ⁻⁸ (C ¹⁸ O)	1.7 × 10 ⁻⁸ (¹⁸ OCO)	3.5 × 10 ⁻¹⁰ (¹⁸ O ₂)	2.8 × 10 ⁻¹² (¹⁸ O ₃)
		34	4.0 × 10 ⁻⁹	—	1.6 × 10 ⁻⁷	—
		59	1.3 × 10 ⁻⁹	—	3.1 × 10 ⁻⁹	—
		63	—	—	2.6 × 10 ⁻⁹	—
		87	—	—	—	—
34	1.1 × 10 ⁻⁹	—	—	4 × 10 ⁻¹⁰		
	1.5 × 10 ⁻⁹	—	—	6.3 × 10 ⁻¹¹		
	2.6 × 10 ⁻⁹ (C ¹⁸ O)	1.0 × 10 ⁻⁸	—	—		
1 : 4	CO ₂ : ¹⁸ O ₂	60–64	4.9 × 10 ⁻¹⁰	—	5.0 × 10 ⁻⁹	—
			5.8 × 10 ⁻¹⁰ (C ¹⁸ O)	—	3.1 × 10 ⁻⁸ (¹⁸ OO)	6.4 × 10 ⁻¹¹ (¹⁸ OO ₂ /O ¹⁸ OO)
			—	—	1.6 × 10 ⁻⁷ (¹⁸ O ₂)	1.8 × 10 ⁻¹⁰ (O ¹⁸ O ₂ / ¹⁸ OO ¹⁸ O)
			—	—	3.1 × 10 ⁻¹⁰	2.0 × 10 ⁻¹⁰ (¹⁸ O ₃)
			—	—	7.8 × 10 ⁻¹⁰ (¹⁸ OO)	1.0 × 10 ⁻¹¹ (¹⁸ OO ₂ /O ¹⁸ OO)
87–88	6.5 × 10 ⁻¹⁰	6.0 × 10 ⁻⁸	1.9 × 10 ⁻⁹ (¹⁸ O ₂)	2.2 × 10 ⁻¹¹ (O ¹⁸ O ₂ / ¹⁸ OO ¹⁸ O)		
	3.7 × 10 ⁻¹⁰ (C ¹⁸ O)	2.7 × 10 ⁻⁹ (¹⁸ OCO)	—	2.3 × 10 ⁻¹¹ (¹⁸ O ₃)		
	—	3.3 × 10 ⁻⁹ (C ¹⁸ O ₂)	—	—		

are the combination bands $\nu_1 + \nu_3$ at 3700 cm^{-1} and $2\nu_2 + \nu_3$ at 3600 cm^{-1} ^{29,30} (Fig. 1b). The $^{13}\text{CO}_2$ isotopomer could be identified from its ν_3 mode at 2280 cm^{-1} and ν_2 mode at 640 cm^{-1} , and also the ^{18}OCO isotopomer *via* the ν_3 stretch at 2331 cm^{-1} .²⁹ The column density of carbon dioxide is found to decrease upon irradiation as monitored through the $\nu_1 + \nu_3$ combination band. During the warm-up program, the mass spectrometer signal associated with carbon dioxide ($m/z = 44$) indicates that this species sublimates around 91–92 K, in good agreement with previous studies.¹⁷

3.1.3 Carbon trioxide. Upon the onset of irradiation, the formation of the C_{2v} isomer of carbon dioxide is readily observed through the ν_1 stretch at 2042 cm^{-1} (Fig. 1c), the ν_2 mode at 1065 cm^{-1} , the ν_3 mode at 973 cm^{-1} (Fig. 1d), and the Fermi resonance at 1890 cm^{-1} . These values are in good agreement with previous studies where they are found to absorb at 2045, 1073, 972, and 1879 cm^{-1} , respectively.³² In addition, the recently identified D_{3h} isomer could also be identified at 1168 cm^{-1} ²¹ (Fig. 1d). Both species remain stable during the isothermal stage, but decompose steadily over temperatures from 51–92 K; this molecular species was not detected by the mass spectrometer ($m/z = 60$).

3.1.4 Other species. We were also able to find evidence for several other species, which include dicarbon monoxide (CCO). Here, the ν_1 fundamental was found to absorb at 1988 cm^{-1} in good agreement with previous studies.³³ We were also able to detect carbon suboxide molecule (C_3O_2), from its ν_3 mode at 2227 cm^{-1} .¹⁶ A weak absorption at 1613 cm^{-1} has been assigned to molecular oxygen based on its appearance when pure oxygen is irradiated.³⁴ Ozone was identified through its ν_3 absorption at 1040 cm^{-1} ³⁵ (Fig. 1d). We were also able to monitor weak signals from a number of oxygen-rich species: CO_4 (C_{2v}) at 1942 cm^{-1} , CO_5 (C_2) at 1914 cm^{-1} , and CO_6 (C_s) at 1878 cm^{-1} in good agreement with previous assignments.^{18–20} In addition, the production of molecular oxygen and its subsequent sublimation was monitored *via* mass spectrometry ($m/z = 32$) where it was found to desorb in four different episodes: (i) at 34 K in agreement with its sublimation temperature within pure oxygen ices,³⁴ (ii) between 49–53 K as carbon monoxide sublimates, (iii) at 70 K whereby a signal was also observed at $m/z = 48$, corresponding to the sublimation of ozone, in agreement with previous studies,³⁴ and (iv) at 91–92 K as the majority of carbon dioxide was found to sublimate.

3.2 $^{13}\text{CO} : \text{C}^{18}\text{O} : \text{CO}_2$ experiments

3.2.1 Carbon monoxide. The ^{13}CO and C^{18}O fundamentals were observed at 2095 and 2087 cm^{-1} , respectively, in agreement with previous studies where they have been found at 2092 and 2089 cm^{-1} ²⁸ (Fig. 1c). The corresponding $2\nu_1$ overtones were isolated at 4162 cm^{-1} and 4156 cm^{-1} . In contrast to experiments carried out using pure $\text{CO} : \text{CO}_2$ ices (Section 3.1), we are here able to monitor the production of carbon monoxide at 2140 cm^{-1} from radiolysis of carbon dioxide separately from the destruction and/or reactions involving the $^{13}\text{CO}/\text{C}^{18}\text{O}$ precursors (Table 2; Fig. 1c). In addition, a smaller band growing at 2041 cm^{-1} during irradiation could be

ascribed to the fundamental of $^{13}\text{C}^{18}\text{O}$. From mass spectroscopy during the warming of the sample (Table 3), we were able to observe all four isotopomers of carbon monoxide (CO at $m/z = 28$, ^{13}CO at $m/z = 29$, C^{18}O at $m/z = 30$, and $^{13}\text{C}^{18}\text{O}$ at $m/z = 31$). A small out-gassing event occurred at around 30 K where only CO was detectable. Two larger sublimation events occurred at 45 K and 47–49 K where all four isotopomers of carbon monoxide were detectable, and correspond to the bulk of CO as well as remaining O_2 sublimation. Signals from all four isotopomers were also detectable during the sublimation of carbon dioxide between 91–92 K; however, the relative contributions of each indicate that CO itself is the most abundant isotopomer by an order of magnitude during this final out-gassing event.

3.2.2 Carbon dioxide. As before, carbon dioxide within the ice prior to radiation could be characterized by infrared absorptions at 1276 (ν_1), 667 , 657 (ν_2), 2334 (ν_3), 1383 ($2\nu_2$), 3705 ($\nu_1 + \nu_3$), and 3599 ($2\nu_2 + \nu_3$) cm^{-1} . The intensity of the combination bands was again observed to decrease during irradiation. Concurrently, the areas of bands identified belonging to $^{13}\text{CO}_2$ at 642 , 639 (ν_2), 2279 (ν_3), 3626 ($\nu_1 + \nu_3$), and 3513 ($2\nu_2 + \nu_3$) cm^{-1} as well as those corresponding to ^{18}OCO at 2327 (ν_3), 3664 ($\nu_1 + \nu_3$), and 3560 ($2\nu_2 + \nu_3$) cm^{-1} were found to increase (Fig. 1b). The ν_3 modes of C^{18}O_2 , $^{18}\text{O}^{13}\text{CO}$, and $^{13}\text{C}^{18}\text{O}_2$ could be identified through absorptions occurring at 2309 , 2262 , and 2243 cm^{-1} , respectively. These results are reflected in the mass spectrometer signals collected during the warm-up of the ice. Here, as carbon dioxide itself sublimated between 91–92 K, all six isotopomers of carbon dioxide were observed: CO_2 ($m/z = 44$), $^{13}\text{CO}_2$ ($m/z = 45$), ^{18}OCO ($m/z = 46$), $^{18}\text{O}^{13}\text{CO}$ ($m/z = 47$), C^{18}O_2 ($m/z = 48$) and $^{13}\text{C}^{18}\text{O}_2$ ($m/z = 49$). The relative abundances are in agreement with the IR observations, in that the most intense signal is from CO_2 , with the signal from $^{13}\text{CO}_2$ and ^{18}OCO almost two orders of magnitude lower. Signals corresponding to $^{18}\text{O}^{13}\text{CO}$ and C^{18}O_2 were detected at levels approximately an order of magnitude further below them, and from $^{13}\text{C}^{18}\text{O}_2$, they were an order of magnitude lower still. Note that additional signals from $^{13}\text{CO}_2$ and ^{18}OCO were detectable during the out-gassing events occurring at 45 and 47–49 K, but the more abundant CO_2 isotopomer was not.

3.2.3 Carbon trioxide. As carbon dioxide is a dominant component of the ice, we expect to observe the C_{2v} form of carbon trioxide around 2045 cm^{-1} , and any ^{18}O substituted isotopomers should be identified down to around 2000 cm^{-1} . Although a broad peak is identified at 2041 cm^{-1} , it is difficult to unambiguously assign this to any specific carrier due to the overlap of the $^{13}\text{C}^{18}\text{O}$ fundamental which occurs at around 2040 cm^{-1} . The $^{13}\text{CO}_3$ (C_{2v}) isotopomer could be positively monitored at 1988 cm^{-1} ; no positive identification of any CO_3 (C_{2v}) features enriched with both ^{13}C and ^{18}O isotopes could be made. The D_{3h} isomer of CO_3 could be identified by a weak peak at 1066 cm^{-1} .

3.2.4 Other species. Also upon irradiation, an absorption associated with molecular oxygen was found at 1612 cm^{-1} (Table 2). Further evidence from mass spectrometry during the warm-up process supports the formation of oxygen as signals

corresponding to O₂ ($m/z = 32$), ¹⁸OO ($m/z = 34$; two orders of magnitude lower), and ¹⁸O₂ ($m/z = 36$; two orders of magnitude lower still) were detected at around 45 K, only slightly higher than in pure oxygen ices, where molecular oxygen sublimates around 40 K.³⁴ Ozone could be characterized from the ν_3 stretch occurring at 1038 cm⁻¹; two additional isotopomers of ozone could also be identified at 1025 cm⁻¹ (¹⁸OO₂) and 1003 (O¹⁸OO).³⁶ The same isotopomers of ozone were confirmed as the only abundant species through mass spectrometry (O₃ at $m/z = 48$, ¹⁸OO₂/O¹⁸OO at $m/z = 50$) as ozone sublimed between 67–68 K. Concurrently, signals from molecular oxygen species (O₂ and ¹⁸OO, but not ¹⁸O₂) are also detected at this time, and are likely fragments produced during the electron impact ionization of the parent ozone species. The determination of other molecular species which may be produced within this ice is hampered by the large number of possible isotopic variants which cause the formation of smaller, broader, indistinct features within the infrared, which could not be uniquely identified.

3.3 CO₂ : C¹⁸O₂ experiments

3.3.1 Carbon monoxide. Here, upon irradiation, both CO and C¹⁸O were observed to be produced as identified through infrared spectroscopy by their fundamental absorptions at 2140 cm⁻¹ and 2089 cm⁻¹, respectively (Table 2; Fig. 1c). Both molecules were produced to a similar abundance, as is evidenced by their almost identical signal intensities ($m/z = 28$, and 30; respectively) within the mass spectrometer during warm-up of the sample, whereby the bulk of carbon monoxide was found to sublime around 47 K (Table 3). Lower intensity signals were also recorded during the sublimation events ascribed to ozone sublimation around 64–72 K, and the sublimation of carbon dioxide occurring around 91 K.

3.3.2 Carbon dioxide. Both the reactants CO₂ and C¹⁸O₂ could be identified through absorptions corresponding to ν_1 (1277 and 1340 cm⁻¹, respectively), ν_2 (668, and 658 as well as 652 and 646 cm⁻¹, respectively), ν_3 (2341 and 2307 cm⁻¹, respectively), $2\nu_2$ (1384 and 1228 cm⁻¹, respectively), $\nu_1 + \nu_3$ (3713 and 3628 cm⁻¹, respectively), and $2\nu_2 + \nu_3$ (3604 and 3519 cm⁻¹, respectively). Upon irradiation, the formation of ¹⁸OCO was observed through transitions corresponding to the ν_3 mode at 2328 cm⁻¹, the $\nu_1 + \nu_3$ combination band at 3663 cm⁻¹, and the $2\nu_2 + \nu_3$ combination band at 3560 cm⁻¹ (Fig. 1b; Table 2). The corresponding ¹³C isotopomers were also identifiable through the ν_3 stretch at 2281 (¹³CO₂), 2264 (¹⁸O¹³CO), and 2246 cm⁻¹ (¹³C¹⁸O₂), as well as from the ν_2 band where ¹³CO₂ was found to absorb at 638 cm⁻¹ and ¹³C¹⁸O₂ was identified at 629 cm⁻¹. From mass spectrometry, signals from carbon dioxide were only observed during the sublimation of this species at 91 K, where CO₂ ($m/z = 44$), C¹⁸O₂ ($m/z = 48$), and ¹⁸OCO ($m/z = 46$) were detected, with the signal of the latter being more than an order of magnitude lower in intensity (Table 3).

3.3.3 Carbon trioxide. Upon irradiation of the sample, it was possible to observe all six expected isotopomers of the C_{2v} structure of carbon trioxide through the strongest ν_1 fundamental where the following assignments could be made: CO₃

at 2045 cm⁻¹, O=C(¹⁸OO) at 2039 cm⁻¹, O=C(¹⁸O₂) at 2031 cm⁻¹, ¹⁸O=C(O₂) at 2025 cm⁻¹, ¹⁸O=C(¹⁸OO) at 2018 cm⁻¹, and finally C¹⁸O₃ at 2008 cm⁻¹ (Fig. 1c; Table 2). Regarding the corresponding D_{3h} isotopomers, which are expected within the region of 1150–1165 cm⁻¹,²¹ a single broad feature was identified in this region, whereby the identification of the underlying isotopomers was not possible.

3.3.4 Other species. Although molecular oxygen could not be detected through infrared spectroscopy, its presence is confirmed through monitoring of the molecular oxygen ion peaks observed with the mass spectrometer as the sample is warmed (Table 3). Here, three separate sublimation events are seen to occur: at 40 K which is associated to the sublimation of molecular oxygen itself, but it is also detected over 64–72 K, and finally during the sublimation of carbon dioxide around 91 K. The latter two signals are thought to arise from fragment ions produced during the electron impact ionization of the ozone and carbon dioxide parent ions, respectively. In each case, the amount of ¹⁸OO ($m/z = 34$) was found to be the most abundant isotopomer formed. Signals associated with ozone was found to sublime around 60–64 K, and during the sublimation of carbon dioxide between 87–88 K. Here, although the signal of the O₃ isotopomer could not be discerned from the stronger signals from C¹⁸O₂ (both $m/z = 48$), the relative intensities of the other isotopomers detected indicate that the isotopically mixed species were found to be an order of magnitude more abundant than their pure counterparts (at least for ¹⁸O₃; $m/z = 54$). Ozone could additionally be characterized from infrared spectroscopy through its ν_3 asymmetric stretch where all six isotopomers could be detected: O₃ (1043 cm⁻¹), ¹⁸OO₂ (1031 cm⁻¹), ¹⁸OO¹⁸O (1023 cm⁻¹), O¹⁸O¹⁸O (1010 cm⁻¹), O¹⁸O₂ (996 cm⁻¹), and ¹⁸O₃ (989 cm⁻¹). Each of these is in accordance with previous assignments in carbon dioxide (Fig. 1d; Table 2).³² No other molecular species could be uniquely identified.

3.4 CO₂ : O₂ experiments

3.4.1 Carbon monoxide. The formation of carbon monoxide was verified through the observation of its fundamental at 2142 cm⁻¹ (Fig. 1c; Table 2), although the overtone band at 4257 cm⁻¹ could also be identified. During the warm-up of the sample, signals from mass spectrometry at $m/z = 28$ indicate that the majority of carbon monoxide was found to sublime at 34 K, with smaller amounts observed around 59 K (just prior to ozone desorption), and also at 87 K (as carbon dioxide sublimates).

3.4.2 Carbon dioxide. Carbon dioxide itself was recognized prior to irradiation through absorptions from transitions appearing at: ν_3 (2357 and 2337 cm⁻¹), ν_2 (667 and 658 cm⁻¹), $2\nu_2$ (1382 cm⁻¹), $\nu_1 + \nu_3$ (3705 cm⁻¹; Fig. 1b), and $2\nu_2 + \nu_3$ (3600 cm⁻¹; Fig. 1b; Table 2). In addition, two isotopomers could be identified from the strongest absorption feature: the ν_3 asymmetric stretch where ¹³CO₂ could be seen at 2280 cm⁻¹ and ¹⁸OCO was found at 2326 cm⁻¹. The only signal identified during the temperature warm-up corresponding to carbon dioxide ($m/z = 44$) was found during the sublimation of this species around 87 K (Table 3).

3.4.3 Carbon trioxide. The cyclic C_{2v} isomer of carbon trioxide was identified through its strongest ν_1 absorption where it was found to absorb at 2044 cm^{-1} (Fig. 1c), and also the Fermi resonance band found at 1896 cm^{-1} (Table 2). Absorptions assigned to the planar D_{3h} isomer are found at 1167 cm^{-1} (Fig. 1d). No signals from these species could be detected through mass spectrometry during the warm-up of the ice sample.

3.4.4 Other species. The fundamental absorption of molecular oxygen could be identified at 1550 cm^{-1} , in accordance to previous studies of pure ices³⁷ (Table 2). Upon irradiation, a second band thought to be associated with this molecule appears around 1610 cm^{-1} . During the warm-up procedure, the majority of molecular oxygen ($m/z = 32$) was found to sublime around 34 K, with smaller amounts being detected around 59 K, and 63 K as ozone sublimates (Table 3). It is likely that this is a fragment produced during the electron impact ionization of from ozone. Ozone itself could be identified within the ice through absorptions occurring at 1107 (ν_1 ; Fig. 1d), 705 (ν_2), 1041 (ν_3 ; Fig. 1d), and 2109 cm^{-1} ($\nu_1 + \nu_3$; Fig. 1c). Signals were detected for this species by mass spectrometry ($m/z = 48$) as it sublimed from the ice around 63 K and during the sublimation of CO_2 at 87 K. Also detectable through infrared spectroscopy are a number of oxygen-rich species also observable in the radiation of pure carbon dioxide ices: CO_4 (C_{2v}) at 1942 cm^{-1} , CO_5 (C_2) at 1913 cm^{-1} , and CO_6 (C_s) at 1879 cm^{-1} (Table 2).

3.5 $\text{CO}_2 : ^{18}\text{O}_2$ experiments

3.5.1 Carbon monoxide. The formation of carbon monoxide was observed through the growth of the fundamental band where it was found to absorb at 2141 cm^{-1} (Fig. 1c; Table 2). The C^{18}O isotopomer at 2090 cm^{-1} appears later on in the radiation (Fig. 1c). The signals from mass spectrometry corresponding to these species (at $m/z = 28$ and 30, respectively) indicate that most of the carbon monoxide sublimates around 34 K. These species were also detected as ozone and carbon dioxide sublime around 60–64 K and 87–88 K, respectively.

3.5.2 Carbon dioxide. Within the ice sample prior to irradiation, absorptions from carbon dioxide were assigned as ν_1 at 1279 cm^{-1} , ν_2 at 660 and 668 cm^{-1} , ν_3 at 2336 and 2359 cm^{-1} , $\nu_1 + \nu_3$ at 3705 cm^{-1} (Fig. 1b), and $2\nu_2 + \nu_3$ at 3601 cm^{-1} (Fig. 1b; Table 2). Also observable *via* the strongest absorption, the ν_3 asymmetric stretch were absorptions originating from ^{18}OCO at 2327 cm^{-1} , and $^{13}\text{CO}_2$ at 2280 cm^{-1} . Upon irradiation, a large increase in the abundance of ^{18}OCO was observed through additional absorptions occurring at 3663 cm^{-1} ($\nu_1 + \nu_3$; Fig. 1b) and 3560 cm^{-1} ($2\nu_2 + \nu_3$; Fig. 1b). It was also possible to observe the $^{18}\text{O}^{13}\text{CO}$ isotopomer from the ν_3 asymmetric stretch at 2262 cm^{-1} . The C^{18}O_2 isotopomer forms later in the irradiation and was observed through bands at 2310 cm^{-1} (ν_3), 3626 cm^{-1} ($\nu_1 + \nu_3$; Fig. 1b), and 3517 cm^{-1} ($2\nu_2 + \nu_3$; Fig. 1b); the latter being also observable prior to irradiation. Due to the large abundance of this species, the corresponding ^{13}C isotopomer, $^{13}\text{C}^{18}\text{O}_2$, is also observable, again through the ν_3 asymmetric stretch at 2244 cm^{-1} . From mass spectrometry, the three

isotopomers of carbon dioxide (CO_2 at $m/z = 44$, ^{18}OCO at $m/z = 46$, and C^{18}O_2 at $m/z = 48$) were all detected only during the sublimation of carbon dioxide at 87–88 K (Table 3).

3.5.3 Carbon trioxide. From Fig. 1c, it is clear that carbon trioxide is formed within this ice where multiple strong absorptions are found within the range of $2000\text{--}2050\text{ cm}^{-1}$, which is the region where the ν_1 fundamental of all the carbon trioxide isotopomers will occur (Section 3.3.3). However, due to overlapping absorptions from other species (not only the fundamental of $^{13}\text{C}^{18}\text{O}$ at around 2040 cm^{-1} , but also the $\nu_1 + \nu_3$ combination band of $^{18}\text{O}_3$ which absorbs at approximately 1995 cm^{-1}), we were unable to unambiguously assign any spectral features to any particular carbon trioxide species in this experiment.

3.5.4 Other species. Prior to irradiation, the molecular oxygen ($^{18}\text{O}_2$) band could be identified through a weak band corresponding to the fundamental appearing at 1463 cm^{-1} (Table 2).³⁸ Upon irradiation, a band at 1508 cm^{-1} becomes visible, and is assigned to the ^{18}OO fundamental. The signals from the mass spectrometer during the warm-up of the sample indicate that molecular oxygen primarily sublimates around 34 K where all three isotopomers are detected, with the $^{18}\text{O}_2$ being most abundant, with ^{18}OO and O_2 being one and two orders of magnitude lower in intensity respectively (Table 3). Each of the isotopomers of molecular oxygen is also detected during the sublimation of ozone around 60–64 K, which are again attributed to molecular fragments formed during the electron impact ionization of the ozone parent ion. Ozone itself could be detected at this time, the strongest signal observed being for $^{18}\text{O}_3$ ($m/z = 54$); almost at the same intensity is the signal at $m/z = 52$, corresponding to ozone isotopomers with a single ^{16}O atom present. The signal at $m/z = 50$, corresponding to ozone isotopomers with two ^{16}O atoms present, is an order of magnitude lower still. Due to the overlap of the O_3 isotopomer, with the stronger signal observed from C^{18}O_2 (both $m/z = 48$), it is difficult to quantify the contribution from this particular species. Within the infrared ice after irradiation, all six isotopomers of ozone could again be identified from the ν_3 asymmetric stretch, however, their frequencies are slightly red-shifted (Fig. 1d): O_3 (1038 cm^{-1}), $^{18}\text{OO}_2$ (1024 cm^{-1}), $^{18}\text{OO}^{18}\text{O}$ (1015 cm^{-1}), $\text{O}^{18}\text{O}^{18}\text{O}$ (1004 cm^{-1}), O^{18}O_2 (991 cm^{-1}), and $^{18}\text{O}_3$ (981 cm^{-1}). In addition, the $\nu_1 + \nu_3$ combination band for $^{18}\text{O}_3$ could be identified at 1995 cm^{-1} (Fig. 1c; Table 2). No other molecular species could be uniquely identified.

4. Discussion

4.1 Kinetic analysis

In this section, we present a brief discussion of the underlying kinetics governing the evolution of the observed carbon monoxide, carbon dioxide, and carbon trioxide species within the isotopic ice mixtures presented here. The $\text{CO} : \text{CO}_2$ and $\text{CO}_2 : \text{O}_2$ ice mixtures will not be discussed, as more mechanistical information is revealed through analysis of their isotopic counterparts. For simplicity, the kinetic analysis has been carried out under the assumption that the production/destruction of each species can be accounted for by a series of

Table 4 Summary of derived rate constants to account for the observed species within the irradiated ice mixtures. For each ice mixture, a reaction scheme is shown to account for the production of each species where the kinetics have been investigated; note that each reaction scheme incorporates either a one, two, or three step sequential formation sequence; the species for which the column density was used for the purpose of fitting is highlighted in bold. The column densities of the reactants, $[A]_0$, are given as column densities (molecules cm^{-2}), and the rate constants in units of s^{-1} . The resulting figure, where the fit can be visualized, is indicated in the last column

Ice mixture	Species	Reaction	Reaction scheme	Column densities/ molecules cm^{-2}	Rate constants/ s^{-1}	Figure
$^{13}\text{CO} : \text{C}^{18}\text{O} : \text{CO}_2$	CO_2	1	$\text{CO}_2 \xrightarrow{k_1} \text{X}$	$[\text{CO}_2]_0 = 5.99 \pm 0.03 \times 10^{17}$	$k_1 = 1.68 \pm 0.21 \times 10^{-5}$	2a
	^{13}CO	2	$^{13}\text{CO} \xrightarrow{k_2} \text{X}$	$[^{13}\text{CO}]_0 = 8.96 \pm 0.01 \times 10^{16}$	$k_2 = 1.19 \pm 0.07 \times 10^{-5}$	2b
	C^{18}O	3	$\text{C}^{18}\text{O} \xrightarrow{k_3} \text{X}$	$[\text{C}^{18}\text{O}]_0 = 8.86 \pm 0.01 \times 10^{16}$	$k_3 = 7.46 \pm 0.60 \times 10^{-6}$	2c
	CO	4	$\text{CO}_2 \xrightarrow{k_4} [\text{CO} \dots \text{O}] \xrightarrow{k_5} \text{X}$	$[\text{CO}_2]_0 = 5.99 \pm 0.03 \times 10^{17}$	$k_4 = 1.52 \pm 0.02 \times 10^{-5}$	2d
				$[\text{CO}]_0 = 2.65 \times 10^{15 \text{ a}}$	$k_5 = 3.05 \pm 0.13 \times 10^{-4}$	
	$^{13}\text{CO}_2$	5	$[^{13}\text{CO} \dots \text{O}] \xrightarrow{k_6, ^{13}\text{CO}_2} \xrightarrow{k_7} \text{X}$	$[^{13}\text{CO}]_0 = 8.96 \pm 0.01 \times 10^{16}$	$k_6 = 2.73 \pm 0.02 \times 10^{-5}$	2e
				$[^{13}\text{CO}_2]_0 = 5.48 \times 10^{15 \text{ a}}$	$k_7 = 4.99 \pm 0.04 \times 10^{-4}$	
$\text{CO}_2 : \text{C}^{18}\text{O}_2$	^{18}OCO	6	$[\text{C}^{18}\text{O} \dots \text{O}] \xrightarrow{k_8, ^{18}\text{OCO}} \xrightarrow{k_9} \text{X}$	$[\text{C}^{18}\text{O}]_0 = 8.86 \pm 0.01 \times 10^{16}$	$k_8 = 3.10 \pm 0.29 \times 10^{-5}$	2f
				$[^{18}\text{OCO}]_0 = 3.20 \times 10^{15 \text{ a}}$	$k_9 = 3.06 \pm 0.75 \times 10^{-4}$	
	$^{13}\text{CO}_3$	7	$[^{13}\text{CO} \dots \text{O}] \xrightarrow{k_6} \xrightarrow{^{13}\text{CO}_2 + \text{O}} \xrightarrow{k_{10}, ^{13}\text{CO}_3} \xrightarrow{k_{11}} \text{X}$	$[^{13}\text{CO}]_0 = 8.96 \pm 0.01 \times 10^{16}$	$k_{10} = 1.57 \pm 0.24 \times 10^{-3}$	2g
					$k_{11} = 1.21 \pm 0.04 \times 10^{-1}$	
	CO_2	8	$\text{CO}_2 \xrightarrow{k'_1} \text{X}$	$[\text{CO}_2]_0 = 2.31 \pm 0.01 \times 10^{17}$	$k'_1 = 5.50 \pm 0.10 \times 10^{-5}$	3a
	C^{18}O_2	9	$\text{C}^{18}\text{O}_2 \xrightarrow{k'_2} \text{X}$	$[\text{C}^{18}\text{O}_2]_0 = 2.49 \pm 0.01 \times 10^{17}$	$k'_2 = 2.64 \pm 0.16 \times 10^{-5}$	3b
	CO	10	$\text{CO}_2 \xrightarrow{k'_3} [\text{CO} \dots \text{O}] \xrightarrow{k'_4} \text{X}$	$[\text{CO}_2]_0 = 2.31 \pm 0.01 \times 10^{17}$	$k'_3 = 1.83 \pm 0.01 \times 10^{-5}$	3c
			$[\text{CO}]_0 = 4.17 \times 10^{13 \text{ a}}$	$k'_4 = 2.43 \pm 0.04 \times 10^{-4}$		
	11	$\text{C}^{18}\text{O}_2 \xrightarrow{k'_5} [\text{C}^{18}\text{O} \dots ^{18}\text{O}] \xrightarrow{k'_6} \text{X}$	$[\text{C}^{18}\text{O}_2]_0 = 2.49 \pm 0.01 \times 10^{17}$	$k'_5 = 1.69 \pm 0.01 \times 10^{-5}$	3d	

Table 4 (continued)

Ice mixture	Species	Reaction	Reaction scheme	Column densities/ molecules cm ⁻²	Rate constants/s ⁻¹	Figure
				[C ¹⁸ O] ₀ = 8.83 × 10 ¹³ ^a	k'₆ = 2.57 ± 0.06 × 10 ⁻⁴	
	¹⁸ OCO	12	$[\text{CO}_2 \dots \text{C}^{18}\text{O}_2] \xrightarrow{k'_7} [\text{CO} \dots \text{O} \dots \text{C}^{18}\text{O} \dots \text{O}^{18}\text{O}]$ $\xrightarrow{k'_8} [\text{CO}_2 \dots \text{C}^{18}\text{O}_2] / [\text{C}^{18}\text{OCO} \dots \text{C}^{18}\text{OCO}] \xrightarrow{k'_9} \text{X}$	[CO₂] ₀ = 2.31 ± 0.01 × 10 ¹⁷ ^b	k'₇ = 8.80 × 10 ⁻⁶ ^c	3e
	CO₃	13	$[\text{CO}_2 \dots \text{CO}_2] \xrightarrow{k'_5} [\text{CO} \dots \text{O} \dots \text{CO}_2] \xrightarrow{k'_{10}} [\text{CO} \dots \text{CO}_3] \xrightarrow{k'_{11}} \text{X}$	[C ¹⁸ O₂] ₀ = 2.49 ± 0.01 × 10 ¹⁷ ^b [¹⁸ OCO] ₀ = 2.12 ± 0.01 × 10 ¹⁵ ^a	k'₈ = 1.44 ± 0.19 × 10 ⁻³ k'₉ = 2.13 ± 0.38 × 10 ⁻⁴ k'₁₀ = 1.77 ± 0.06 × 10 ⁻³	3f
	OC ¹⁸ OO	14	$[\text{C}^{18}\text{O}_2 \dots \text{CO}_2] \xrightarrow{k'_5} [\text{C}^{18}\text{O} \dots \text{O} \dots \text{CO}_2] \xrightarrow{k'_{12}} [\text{CO} \dots \text{OC}^{18}\text{OO}] \xrightarrow{k'_{13}} \text{X}$	[CO₂] ₀ = 2.31 ± 0.01 × 10 ¹⁷	k'₁₁ = 3.48 ± 0.03 × 10 ⁻² k'₁₂ = 1.54 ± 0.06 × 10 ⁻³	3g
	¹⁸ OCO₂	15	$[\text{C}^{18}\text{O}_2 \dots \text{CO}_2] \xrightarrow{k'_5} [\text{C}^{18}\text{O} \dots \text{O} \dots \text{CO}_2] \xrightarrow{k'_{14}} [\text{CO} \dots \text{C}^{18}\text{OCO}_2] \xrightarrow{k'_{15}} \text{X}$	[CO₂] ₀ = 2.31 ± 0.01 × 10 ¹⁷	k'₁₃ = 3.78 ± 0.04 × 10 ⁻² k'₁₄ = 1.01 ± 0.07 × 10 ⁻³	3h
	OC ¹⁸ O₂	16	$[\text{CO}_2 \dots \text{C}^{18}\text{O}_2] \xrightarrow{k'_5} [\text{CO} \dots \text{O} \dots \text{C}^{18}\text{O}_2] \xrightarrow{k'_{16}} [\text{CO} \dots \text{OC}^{18}\text{O}_2] \xrightarrow{k'_{17}} \text{X}$	[C ¹⁸ O₂] ₀ = 2.49 ± 0.01 × 10 ¹⁷	k'₁₅ = 8.80 ± 0.20 × 10 ⁻² k'₁₆ = 1.41 ± 0.08 × 10 ⁻³	3i
	¹⁸ OC ¹⁸ OO	17	$[\text{CO}_2 \dots \text{C}^{18}\text{O}_2] \xrightarrow{k'_3} [\text{CO} \dots \text{O} \dots \text{C}^{18}\text{O}_2] \xrightarrow{k'_{18}} [\text{CO} \dots \text{C}^{18}\text{OC}^{18}\text{OO}] \xrightarrow{k'_{19}} \text{X}$	[C ¹⁸ O₂] ₀ = 2.49 ± 0.01 × 10 ¹⁷	k'₁₇ = 9.47 ± 0.14 × 10 ⁻² k'₁₈ = 1.59 ± 0.06 × 10 ⁻³	3j
	C ¹⁸ O₃	18	$[\text{C}^{18}\text{O}_2 \dots \text{C}^{18}\text{O}_2] \xrightarrow{k'_5} [\text{C}^{18}\text{O} \dots \text{O} \dots \text{C}^{18}\text{O}_2] \xrightarrow{k'_{20}} [\text{C}^{18}\text{O} \dots \text{C}^{18}\text{O}_3] \xrightarrow{k'_{21}} \text{X}$	[C ¹⁸ O₂] ₀ = 2.49 ± 0.01 × 10 ¹⁷	k'₁₉ = 4.39 ± 0.04 × 10 ⁻² k'₂₀ = 1.79 ± 0.06 × 10 ⁻³	3k
CO₂ : ¹⁸ O₂	CO₂	19	$\text{CO}_2 \xrightarrow{k''_1} \text{X}$	[CO₂] ₀ = 8.99 ± 0.08 × 10 ¹⁶	k'₂₁ = 4.31 ± 0.03 × 10 ⁻²	4a
	CO	20	$\text{CO}_2 \xrightarrow{k''_2} [\text{CO} \dots \text{O}] \xrightarrow{k''_3} \text{X}$	[CO₂] ₀ = 8.99 ± 0.08 × 10 ¹⁶	k''₁ = 4.28 ± 0.07 × 10 ⁻⁴ k''₂ = 1.58 ± 0.02 × 10 ⁻⁴ k''₃ = 8.92 ± 0.09 × 10 ⁻⁴	4b

Table 4 (continued)

Ice mixture	Species	Reaction	Reaction scheme	Reaction scheme	Column densities/ molecules cm ⁻²	Rate constants/s ⁻¹	Figure
	¹⁸ OCO	21	$[\text{CO}_2 \dots ^{18}\text{O}] \xrightarrow{k_4''} [^{18}\text{OCO} \dots \text{O}] \xrightarrow{k_5''} \text{X}$		$[\text{CO}_2]_0 = 8.99 \pm 0.08 \times 10^{16}$	$k_4'' = 1.47 \pm 0.04 \times 10^{-4}$ $k_5'' = 3.72 \pm 0.19 \times 10^{-4}$	4c
	C ¹⁸ O	22	$[\text{CO}_2 \dots ^{18}\text{O}] \xrightarrow{k_4''} [^{18}\text{OCO} \dots \text{O}] \xrightarrow{k_6''} [\text{C}^{18}\text{O} \dots \text{O}] \xrightarrow{k_7''} \text{X}$		$[\text{CO}_2]_0 = 8.99 \pm 0.08 \times 10^{16}$	$k_6'' = 3.71 \pm 0.08 \times 10^{-4}$ $k_7'' = 8.42 \pm 0.19 \times 10^{-4}$	4d
	C ¹⁸ O ₂	23	$[\text{CO}_2 \dots 2^{18}\text{O}] \xrightarrow{k_4''} [^{18}\text{OCO} \dots ^{18}\text{O} \dots \text{O}] \xrightarrow{k_6''} [\text{C}^{18}\text{O}_2 \dots \text{O}] \xrightarrow{k_8''} \text{X}$		$[\text{CO}_2]_0 = 8.99 \pm 0.08 \times 10^{16}$	$k_8'' = 7.82 \pm 0.33 \times 10^{-4}$	4e
					$[\text{C}^{18}\text{O}_2]_0 = 1.70 \times 10^{15} \text{ }^a$	$k_9'' = 8.78 \pm 3.76 \times 10^{-4}$	

^a This is the amount of this species present prior to irradiation, and is added to the fit as a constant. ^b The amount of $[A]_0$ according to eqn (3) is given here as $[A]_0 = [\text{CO}_2]_0 + [\text{C}^{18}\text{O}_2]_0$ to account for both reactants acting as possible precursors. ^c The rate constant used here is the average from k_4'' and k_5'' .

sequential reactions. Each of the species has therefore been fit using a one ($\text{A} \xrightarrow{k_a} \text{X}$), two ($\text{A} \xrightarrow{k_a} \text{B} \xrightarrow{k_b} \text{X}$), or three ($\text{A} \xrightarrow{k_a} \text{B} \xrightarrow{k_b} \text{C} \xrightarrow{k_c} \text{X}$) step mechanism where in every case the last step includes a reaction/destruction pathway to an unspecified species 'X' to account for additional reactions that may be occurring within the ice. The rate constants for each reaction step are here denoted as k_a , k_b , and k_c , and the bold letter represents the species for which the profile has been used to produce the fit. Table 4 compiles the rate constants identified for each reaction listed to account for the temporal profiles of species present for the ice mixtures under study whereby those related to the $\text{CO}_2 : \text{C}^{18}\text{O}_2$ system and $\text{CO}_2 : ^{18}\text{O}_2$ system have been denoted with single (k') and double (k'') primes to distinguish them from those derived for the $^{13}\text{CO} : \text{C}^{18}\text{O} : \text{CO}_2$ system. The position of the bold species within the 'reaction scheme' column indicates which type of fit has been used in each case. The rate equations for one, two, and three step mechanisms are shown as eqn (1)–(3):³⁹

$$[A]_t = [A]_0 e^{-k_a t} \quad (1)$$

$$[B]_t = \frac{k_a [A]_0}{k_b - k_a} (e^{-k_a t} - e^{-k_b t}) \quad (2)$$

$$[C]_t = \left[\frac{k_a k_b [A]_0}{(k_b - k_a)(k_c - k_a)} \right] e^{-k_a t} + \left[\frac{k_a k_b [A]_0}{(k_a - k_b)(k_c - k_b)} \right] e^{-k_b t} + \left[\frac{k_a k_b [A]_0}{(k_a - k_c)(k_b - k_c)} \right] e^{-k_c t} \quad (3)$$

In each case, the column density, $[A]_0$, is set to that of the appropriate reactants, and derived rate constants will be preserved if they were evaluated in previous steps. We shall now summarize the results of the kinetic analysis of each system in turn.

4.1.1 ¹³CO : C¹⁸O : CO₂ system. Fig. 2 shows the temporal evolution of the column densities for each species investigated here, as determined from integration of the areas of their infrared absorptions during the irradiation process, along with the results of the kinetic fits, the results of which are summarized in Table 4 (reactions (1)–(7)). First, let us consider the temporal profile of CO₂, which was produced through integration of the $2\nu_2 + \nu_3$ combination band at 3599 cm⁻¹ using an integral absorption coefficient of 4.5×10^{-19} cm molecule⁻¹.²⁵ Here, it was assumed the profile would follow simple exponential decay ($\text{A} \rightarrow \text{X}$) which was used to fit the temporal profile of this species (Fig. 2a; Table 4, reaction (1)). This accounts for the total destruction of this species either through radiolysis-induced dissociation (e.g. $\text{CO}_2 \rightarrow \text{CO} + \text{O}$) or any reaction this species participates in (e.g. $\text{CO}_2 + \text{O} \rightarrow \text{CO}_3$). The temporal profiles for ¹³CO and C¹⁸O were produced from integration of their fundamental bands at 2095 and 2087 cm⁻¹ using the integral absorption coefficient of 1.1×10^{-17} cm molecule⁻¹.²⁵ The profiles for these reactants were also assumed to follow an exponential decay, as they are expected to also undergo radiolysis-induced reaction/dissociation as well as reaction with suprathreshold oxygen atoms produced from the dissociation of carbon dioxide (Fig. 2b and c; Table 4, reactions

(2) and (3)). Considering next, the production of CO, this was monitored through the fundamental band appearing at 2140 cm^{-1} . Here, we consider that the major production pathway of this species is the radiolysis-induced dissociation of CO_2 ($\text{CO}_2 \rightarrow \text{CO} + \text{O}$); once produced, the carbon monoxide species should react in a similar manner to the other $^{13}\text{CO}/\text{C}^{18}\text{O}$ isotopomers (*i.e.* undergo further reaction/destruction). For this reason, this species was fit using a two-step sequential mechanism ($\text{A} \rightarrow \text{B} \rightarrow \text{X}$). The results here are shown in Fig. 2d and Table 4 (reaction (4)). Note that due to a small presence of this species prior to irradiation, a baseline value of $2.65 \times 10^{15}\text{ molecules cm}^{-2}$ was added to the column density of this species during the fitting procedure. The temporal profiles of $^{13}\text{CO}_2$ and ^{18}OCO were taken from integration of the ν_3 fundamental at 2279 cm^{-1} , and the $\nu_1 + \nu_3$ combination band at 3664 cm^{-1} , using absorption coefficients of $7.6 \times 10^{-17}\text{ cm molecule}^{-1}$ and $1.4 \times 10^{-18}\text{ cm molecule}^{-1}$, respectively.²⁵ Due to their presence in the ice sample prior to irradiation (from the gas cylinder), a baseline value of 5.5 and $3.2 \times 10^{15}\text{ molecules cm}^{-2}$ was added to the column densities of $^{13}\text{CO}_2$ and ^{18}OCO , respectively. The production of both $^{13}\text{CO}_2$ and ^{18}OCO are assumed to form through the reaction of the carbon monoxide reactants $^{13}\text{CO}/\text{C}^{18}\text{O}$ with suprathreshold oxygen atoms produced from the radiolysis-induced dissociation of carbon dioxide ($^{13}\text{CO} + \text{O} \rightarrow ^{13}\text{CO}_2$; $\text{C}^{18}\text{O} + \text{O} \rightarrow ^{18}\text{OCO}$). Since suprathreshold oxygen atoms are borne with excess kinetic energy (and may also be electronically excited), they are able to be mobile in the ice, and are able to overcome reaction barriers (in the case of ground state oxygen atoms) to react with carbon monoxide, forming the respective carbon dioxide isotopomers. The reaction of suprathreshold oxygen atoms with carbon monoxide to form carbon dioxide has previously been demonstrated to follow pseudo-first order kinetics.¹⁷ Once the $^{13}\text{CO}_2$ and ^{18}OCO molecules have been produced, it is again presumed that they will participate in further reactions, or undergo radiolysis-induced dissociation, similar to CO_2 . In both cases, the temporal profile was fit assuming a two-step sequential mechanism ($\text{A} \rightarrow \text{B} \rightarrow \text{X}$), the results can be seen in Fig. 2e and f; Table 4, reactions (5) and (6). Lastly, we consider the formation of the carbon trioxide species $^{13}\text{CO}_3$ ($\text{C}_{2\nu}$), which was monitored through the ν_1 fundamental at 1988 cm^{-1} , using an integral absorption coefficient of $8.9 \times 10^{-17}\text{ cm molecule}^{-1}$.¹⁷ This species is assumed to be produced *via* the recombination of a suprathreshold oxygen atom with a previously formed $^{13}\text{CO}_2$ species, and can thus be fit using a three step sequential mechanism ($\text{A} \rightarrow \text{B} \rightarrow \text{C} \rightarrow \text{X}$), which again may subsequently be degraded or participate in further reactions. The result of this fit can be seen in Fig. 2g, and also Table 4, reaction (7).

4.1.2 $\text{CO}_2 : \text{C}^{18}\text{O}_2$ system. For each species investigated kinetically, the temporal evolution of the column density, as well as the results of the kinetic fitting procedure, is shown in Fig. 3, and the results are listed in Table 4 (reactions (8)–(18)). For both the reactants, CO_2 and C^{18}O_2 , the temporal profiles were produced from averaging the column densities derived from the $\nu_1 + \nu_3$ and $2\nu_2 + \nu_3$ combination bands, as well as the ν_3 fundamental from the corresponding ^{13}C isotopomer (subsequently multiplied by 100/1.1 to account for the abundance of ^{13}C relative to ^{12}C). This procedure gives a more accurate

estimation of the column density, which could not reliably be taken from one band due to the fact that the absorption coefficients for the combination bands were found to change upon irradiation. As before (Section 4.1.1.), we assume that the temporal profile of both carbon dioxide reactants should follow an exponential decay due to a combination of their destruction through radiolysis-induced dissociation (*e.g.* $\text{CO}_2 \rightarrow \text{CO} + \text{O}$, $\text{C}^{18}\text{O}_2 \rightarrow \text{C}^{18}\text{O} + ^{18}\text{O}$), and any further reactions involving this molecular species. The results of this fitting procedure for CO_2 and C^{18}O_2 are shown in Fig. 3a and b, as well as Table 4, reactions (8) and (9), respectively. The temporal profiles of CO and C^{18}O were produced from integration of their fundamental bands at 2140 and 2089 cm^{-1} respectively. These species are thought to be primarily produced from the dissociation of CO_2 and C^{18}O_2 , correspondingly. Once they are produced from this initial step, it is again assumed that they may then participate in further reactions, or be degraded upon irradiation. For this reason, they have been fit using a two-step sequential mechanism; the results are shown in Fig. 3c and d, Table 4, reactions (10) and (11). Note that to account for their presence prior to irradiation, 4.17 and $8.83 \times 10^{15}\text{ molecules cm}^{-2}$ were added to the baselines of the CO and C^{18}O column densities during the fitting procedure. The temporal profile of ^{18}OCO was averaged from the derived column densities of the $\nu_1 + \nu_3$ combination band at 3663 cm^{-1} , and the ν_3 fundamental from the corresponding ^{13}C isotopomer at 2264 cm^{-1} (multiplied by 100/1.1). In this case, it was assumed that the dominant pathway to form this molecule was from recombination of CO, or C^{18}O with a suprathreshold O or ^{18}O atom, which was previously generated through reactions (10) and (11) (Table 4). Thus, we attempted to fit this profile using a three-step sequential mechanism. Here, we note that the precursor molecule could potentially be either CO_2 , or C^{18}O_2 so the amount of $[A]_0$ was chosen as the combined column densities of these two species. Here, as the first step is the generation of CO and C^{18}O through reactions (10) and (11) (Table 4), the rate constant taken for this first step (denoted k'_7 in Table 4) was initially taken as the sum of k'_3 and k'_4 . However, if we assume that there is an equal probability of an O or ^{18}O atom adding to either a CO, or C^{18}O molecule, we can conclude that there should be a 50% chance of forming ^{18}OCO , and a 25% chance of forming either CO_2 , or C^{18}O_2 . To take into account the probability of forming ^{18}OCO from the proposed reactants, the value of k'_7 was also halved. The formation of the carbon monoxide precursor and the generation of suprathreshold oxygen atoms/formation of carbon dioxide are treated as two sequential steps ($\text{A} \rightarrow \text{B} \rightarrow \text{C} \rightarrow \text{X}$); any further reactions/degradation of this species is accounted for in the final step (Fig. 3e; Table 4, reaction (12)).

The temporal profiles for the detected isotopomers of CO_3 ($\text{C}_{2\nu}$) were each generated from integration of the ν_1 fundamentals at 2045 (CO_3), 2039 (OC^{18}OO), 2031 (OC^{18}O_2), 2025 ($^{18}\text{OCO}_2$), 2018 ($^{18}\text{OC}^{18}\text{OO}$), and 2008 cm^{-1} (C^{18}O_3). Kinetically, these species were treated in a manner whereby no distinction was made as to whether or not the oxygen atom is able to add solely to the carbon–oxygen bond, or to the carbon atom directly *via* an intermediate cyclic CO_3 (D_{3h}) structure. Part of the reason for taking this approach is the fact that the $^{18}\text{OCO}_2$ and OC^{18}O_2 isotopomers are shown to form at the onset of irradiation, while the column density of ^{18}OCO

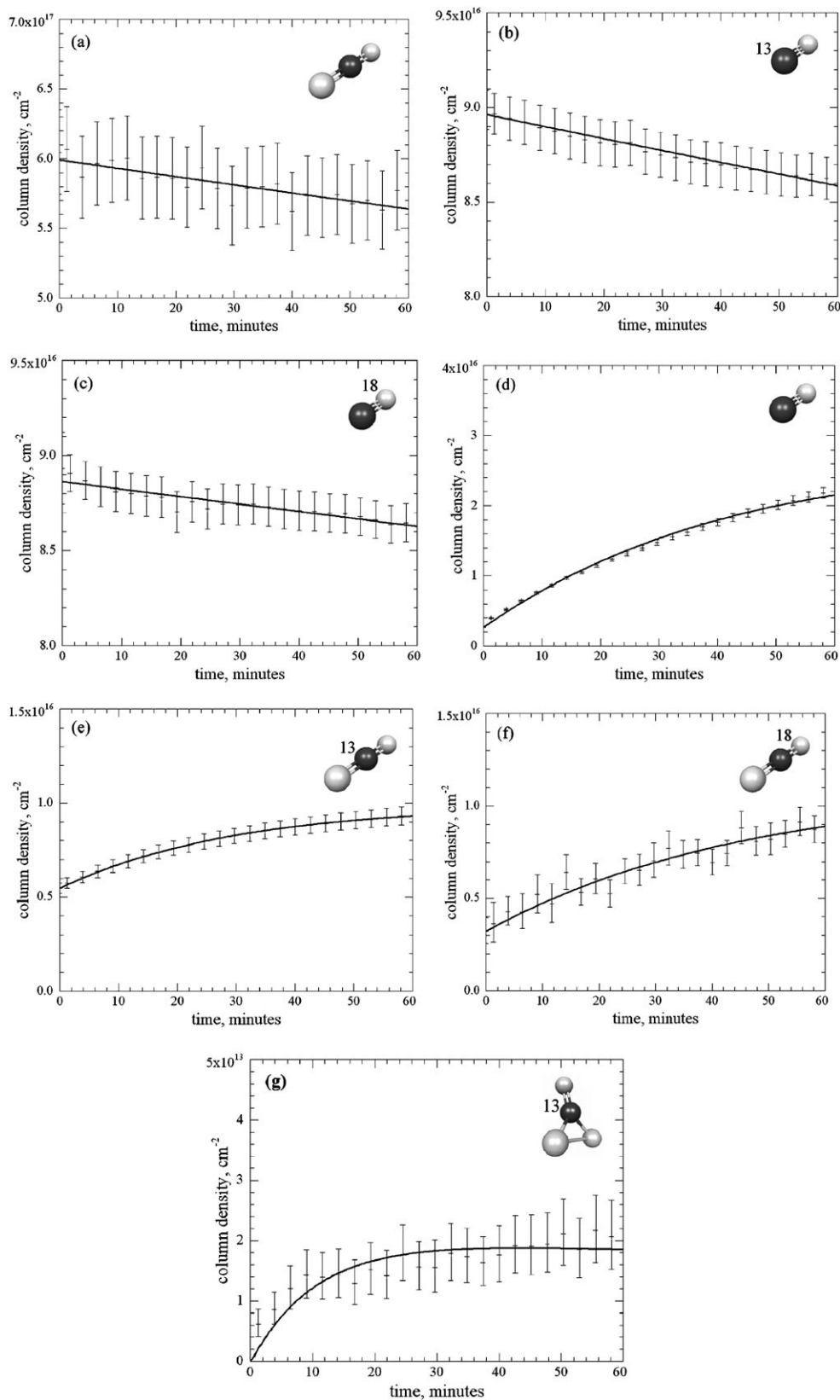


Fig. 2 Temporal evolution of the column densities during the irradiation of $^{13}\text{CO} : \text{C}^{18}\text{O} : \text{CO}_2$ ices for: (a) CO_2 , (b) ^{13}CO , (c) C^{18}O , (d) CO , (e) $^{13}\text{CO}_2$, (f) ^{18}OCO , and (g) $^{13}\text{CO}_3$. Error bars are one standard deviation from the Gaussian fitting procedure, except for (d) and (e) where an error of 5% is indicated. For (d), (e), and (f), column densities of 2.7 , 5.5 , and 3.2×10^{15} molecules cm^{-2} were added to the fits to account for their abundance within the ice prior to irradiation, respectively.

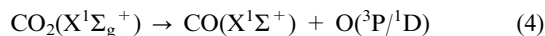
which could feasibly provide additional pathways to form these molecules, by reaction with O and ^{18}O , respectively, was found to only become significant at later stages of irradiation. The precursor species was taken as either CO_2 for the isotopomers containing two ^{16}O atoms, and C^{18}O_2 for the isotopomers containing two ^{18}O atoms. It is assumed that the rate constants for the generation of suprathreshold ^{16}O and ^{18}O atoms are determined from reactions (10) and (11), respectively; strictly, this may depend on a different reactant column density than $[A]_0$, however, as the column densities for both CO_2 and C^{18}O_2 are almost identical, the error introduced here is negligible. As before, the addition of the suprathreshold oxygen atom to the carbon dioxide reactant is taken as a second step, and the further reaction/destruction is added as a last step ($\text{A} \rightarrow \text{B} \rightarrow \text{C} \rightarrow \text{X}$). The results of the fitting procedure for the isotopomers of CO_3 ($\text{C}_{2\nu}$) are shown in Fig. 3f–k, and Table 4, reactions (13)–(18).

4.1.3 $\text{CO}_2 : ^{18}\text{O}_2$ system. Fig. 4 shows the temporal profiles of the column densities for each species investigated. We consider, first, the temporal profile of CO_2 , which was produced from integration of the $2\nu_2 + \nu_3$ combination band at 3601 cm^{-1} . As before, it was assumed that this species could be fit using an exponential decay ($\text{A} \rightarrow \text{X}$), as it is destroyed through either radiolysis-induced dissociation, or reaction; the results of this fitting procedure can be seen in Fig. 4a, and Table 4, reaction (19). The temporal profile of CO was produced from the fundamental band appearing at 2141 cm^{-1} . It was assumed that this species was formed from the radiolysis-induced dissociation of carbon dioxide. An additional pathway was included to account for additional destruction/reactions of this species ($\text{A} \rightarrow \text{B} \rightarrow \text{X}$). The results can be seen in Fig. 4b; Table 4, reaction (20). The temporal profile of ^{18}OCO was monitored through the $2\nu_2 + \nu_3$ combination band at 3560 cm^{-1} . Under the assumption that this molecule is formed from the addition of suprathreshold ^{18}O atoms to CO previously formed under reaction (20) (Table 4), we attempted to fit this temporal profile using a three-step mechanism ($\text{A} \rightarrow \text{B} \rightarrow \text{C} \rightarrow \text{X}$), however, the reaction proceeds so quickly that for the purpose of quantification, and to facilitate further analysis, the first two steps were combined into a pseudo-first order step ($\text{A} \rightarrow \text{B} \rightarrow \text{X}$). The results of this fitting procedure are shown in Fig. 4c as well as Table 4, reaction (21). The temporal profile of the C^{18}O molecule was produced from the fundamental band appearing at 2090 cm^{-1} . Here, we assumed that the ^{18}OCO molecular species previously generated was subsequently dissociated through radiolysis, giving a pseudo-three step mechanism ($\text{A} \rightarrow \text{B} \rightarrow \text{C} \rightarrow \text{X}$), in which B is the ^{18}OCO molecule produced through reaction (20) and the rate constant k_4'' was used (Fig. 4d; Table 4, reaction (22)). Lastly, the profile of the C^{18}O_2 molecule was characterized using the $2\nu_2 + \nu_3$ combination band at 3517 cm^{-1} ; a value of $1.70 \times 10^{15}\text{ molecules cm}^{-2}$ was added to the column density of this species, to account for the presence of this molecule within the ice sample prior to irradiation. As for the production of ^{18}OCO , we found that in the case of C^{18}O_2 , although the production of C^{18}O was deemed a necessary precursor, we were able to fit the temporal profile using a pseudo-three step mechanism ($\text{A} \rightarrow \text{B} \rightarrow \text{C} \rightarrow \text{X}$) based on the production of ^{18}OCO (B in the reaction scheme), again,

utilizing the rate constant k_4'' . The results of this fit are shown in Fig. 4e, and Table 4, reaction (23).

4.2 Summary of key reactions identified

4.2.1 Radiolysis-induced dissociation. As carbon dioxide is the only constituent of the $\text{CO}_2 : \text{C}^{18}\text{O}_2$ ices covered in this study, let us consider the dissociation pathway for this species first. The initial products produced upon radiolysis are carbon monoxide, and atomic oxygen as shown in eqn (4):

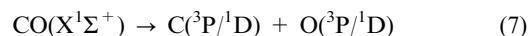


As stated in ref. 17, it is difficult to comment on the precise nature of the excited states produced here compared to what has been detected experimentally elsewhere (see ref. 40). However, the production of ground state carbon monoxide can be readily observed through the detection of both the CO and C^{18}O fundamental bands which occur at 2140 cm^{-1} and 2089 cm^{-1} , respectively (Fig. 1c; Table 2). The relative distributions of O/ ^{18}O atoms as detected through mass spectrometry for the isotopomers of molecular oxygen (Table 3) and ozone (also observable through the ν_3 stretch; Fig. 1d, Tables 2 and 3) are also consistent with this mechanism.

Two key reactions have been suggested to occur during the radiolysis of pure carbon monoxide ices subjected to energetic electrons. There is evidence of chemical processing of pure carbon monoxide ices by photons which are below the energy required to dissociate the molecule,^{41,42} whereas little processing is found to occur when carbon monoxide isolated within a nitrogen matrix is subjected to the same irradiation.⁴³ Thus, it was suggested⁴⁴ that, the underlying mechanism involves the generation of an excited electronic state which can then react with a neighboring carbon monoxide species to yield carbon dioxide and a carbon atom as shown in eqn (5) and (6):



As energetic electrons are also capable of electronic excitation of carbon monoxide,⁴⁵ it is reasonable to assume that this pathway can also occur within ices processed by energetic electrons.^{16,46} Further support for this reaction mechanism comes from the identified products reported by ref. 16; linear carbon chains such as C_3 and C_6 , linear carbon oxide chains of the series C_nO ($n = 2-7$) as well as of the series C_nO_2 ($n = 3-5$, and 7). The non-detection of molecular oxygen or ozone within these experiments indicates that free oxygen is not produced initially from the carbon monoxide reactant. This should be the case if the second feasible pathway occurs to any appreciable extent; dissociation into carbon and oxygen atoms as depicted in eqn (7):



The production of these fragments has been experimentally established where molecular beams of carbon monoxide are bombarded by energetic electrons.⁴⁷ However, when ices containing $\text{CO} : ^{18}\text{O}_2$ were subjected to 5 keV electrons, the first order production of molecules containing C and O atoms suggests their availability from the start of the irradiation process, indicating that eqn (7) is occurring to some extent.²⁴ Within the $\text{CO} : \text{CO}_2$ and $^{13}\text{CO} : \text{C}^{18}\text{O} : \text{CO}_2$ experiments

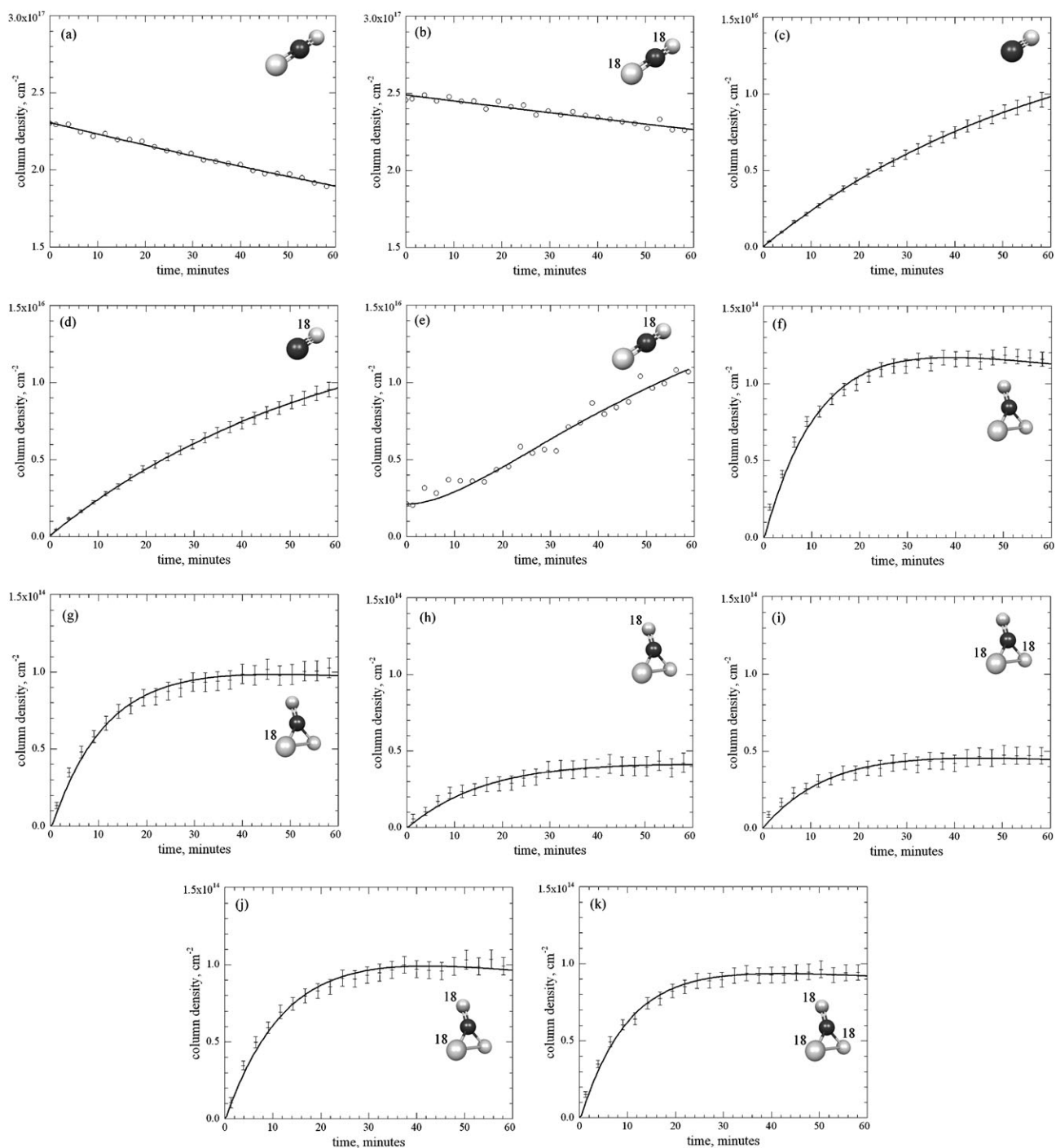
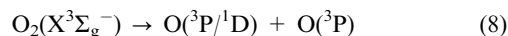


Fig. 3 Temporal evolution of the column densities during the irradiation of CO_2 : C^{18}O_2 ices for: (a) CO_2 , (b) C^{18}O_2 , (c) CO , (d) C^{18}O , (e) ^{18}OCO , (f) CO_3 , (g) OC^{18}OO , (h) $^{18}\text{OCOO}$, (i) OC^{18}O_2 , (j) $^{18}\text{OC}^{18}\text{OO}$, and (k) C^{18}O_3 . Error bars are one standard deviation from the Gaussian fitting procedure, except for (c) and (d) where an error of 5% is indicated. Error bars have been removed from (a), (b), and (e) for clarity. For (e) a value of 1.4×10^{15} molecules cm^{-2} was added to the fit to account for the amount of this species present prior to irradiation.

conducted here, the specific mechanism for carbon monoxide dissociation could not be deciphered, as other reaction mechanisms could account for the observed species produced (Table 4).

Lastly, considering the dissociation of molecular oxygen, it has been assumed that this species dissociates through the

generation of atomic oxygen atoms which, in addition to bearing excess kinetic energy, may also be electronically excited.^{34,40}



Within the CO_2 : O_2 and CO_2 : $^{18}\text{O}_2$ irradiated ices, the availability of ^{16}O and ^{18}O atoms upon the onset of irradiation

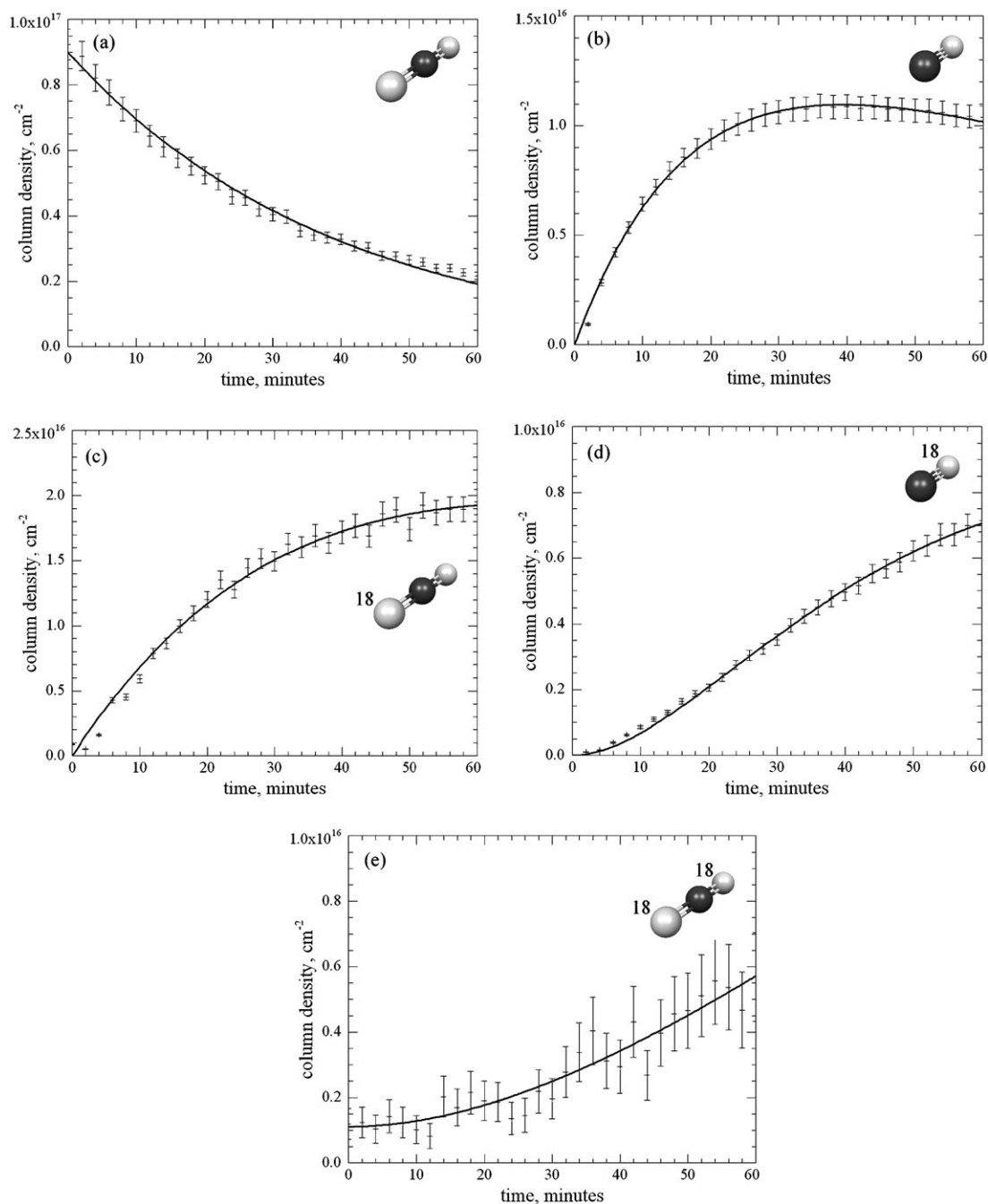


Fig. 4 Temporal evolution of the column densities during the irradiation of $\text{CO}_2 : ^{18}\text{O}_2$ ices for: (a) CO_2 , (b) CO , (c) ^{18}OCO , (d) C^{18}O , and (e) C^{18}O_2 . Error bars shown are 5% of the derived column density with the exception of (e) where 20% is indicated. For (e) a value of 1.2×10^{15} molecules cm^{-2} was added to the fit to account for the amount of this species present prior to irradiation.

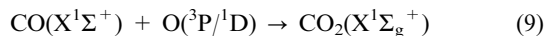
can be seen by the production of O_3 and $^{18}\text{O}_3$ species as monitored in the infrared through the first order appearance of their characteristic ν_3 modes occurring at 1041 and 981 cm^{-1} , respectively (Fig. 1d; Table 2). As discussed previously,³⁴ this reaction readily occurs to produce ozone when the addition of an $\text{O}(^3\text{P})$ atom to molecular oxygen when pure molecular oxygen ices exposed to 5 keV electrons.

4.2.2 Addition of suprathermal oxygen atoms. The dissociation of carbon dioxide, carbon monoxide, and molecular

oxygen can lead to the generation of suprathermal oxygen atoms as outlined in eqn (4), (7) and (8) respectively. The kinetic energy of the oxygen atoms produced is of the order of typically a few eV,^{48,49} and is therefore not in thermal equilibrium with the surrounding ice ($1 \text{ eV} = 11\,604.5 \text{ Kelvin}$); this energy can be utilized to overcome reaction barriers inaccessible at 10 Kelvin . In addition, the suprathermal oxygen atoms produced may also be electronically excited (see ref. 40 for details), supplying additional available energy, access to potential energy surfaces of different multiplicities leading to

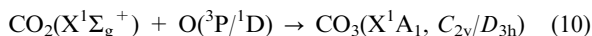
otherwise inaccessible products, and in some cases, the removal of reaction barriers due to differing occupations of atomic orbitals from the ground state configuration.⁵⁰

The formation of carbon dioxide through the reaction of suprathemal oxygen atoms with carbon monoxide as shown in eqn (9) has recently been discussed in detail:²⁴



While no barrier exists for the reaction involving (¹D) oxygen atoms, a barrier of around 49 kJ mol⁻¹ (0.26 eV) has been calculated for reaction with ground state oxygen atoms and may lead to an initially excited state of carbon dioxide.⁵¹ The only strong evidence for this reaction occurring is found during irradiation of the ¹³CO : C¹⁸O : CO₂ ice mixture. Here, the first order generation of ¹³CO₂ and ¹⁸OCO could be explained by the suprathemal addition of oxygen atoms formed through eqn (4) reacting with the ¹³CO and C¹⁸O reactants, respectively (Fig. 2e and f; Table 4, reactions (5) and (6)). The alternative production of carbon dioxide through eqn (6) should lead to equal production of not only ¹³CO₂ and ¹⁸OCO, but also ¹⁸O¹³CO and C¹⁸O₂, which was not observed here. This pathway was therefore also taken as the pathway for the production of ¹⁸OCO within the CO₂ : C¹⁸O₂ ices (Table 4, reaction (12)), and for the formation of ¹⁸OCO and C¹⁸O₂ within CO₂ : ¹⁸O₂ ices (Table 4, reactions (21) and (23)).

The analogous formation of carbon trioxide through reaction of suprathemal oxygen reactions with carbon dioxide is shown in eqn (10):



In this case, reaction with O(¹D) atoms involves a small barrier which lies below the energy of the reactants according to high-level electronic structure calculations calculated in ref. 52, thus both the C_{2v} and D_{3h} isomers should be accessible. They were also able to locate a crossing point on the singlet–triplet potential energy surfaces located 149 kJ mol⁻¹ (1.54 eV) above the reactants, indicating that reactions with suprathemal ground state atoms may also occur. Infrared spectroscopy was used to verify the formation of both C_{2v} and D_{3h} isomers of carbon trioxide each ice irradiation experiment performed (Table 4). During the irradiation of CO₂ : C¹⁸O₂ ices, all six expected isotopomers of the C_{2v} structure could be uniquely identified (Table 4). The kinetic modeling of both ¹⁸OCO₂ and OC¹⁸O₂ isotopomers (Fig. 3h and i; Table 4, reactions (15) and (16)) of the C_{2v} structure indicates that some degree of isomerization between the C_{2v} and D_{3h} structures may occur before either structure is stabilized by the surrounding ice matrix—the barrier to isomerization between these species is calculated to be only 7 kJ mol⁻¹ (0.07 eV).⁵² The higher oxide species detected such as CO₄ (C_{2v}), CO₅ (C₂), and CO₆ (C_s) are also formed from the reaction of the corresponding predecessor with suprathemal oxygen atoms.

4.3 Astrophysical implications

While carbon monoxide and carbon dioxide are known components of interstellar ices, carbon trioxide has yet to be positively identified. It is highly likely that in processed interstellar ices rich in carbon dioxide, carbon trioxide is likely to form, possibly in concentrations high enough to be detected

astronomically. As has been discussed in ref. 53, the strongest band of this molecule overlaps with that of the OCS molecule, which has been previously assigned to the carrier of a band at 2041 cm⁻¹ (4.9 μm) as detected towards the high-mass protostar W33A.^{54,55} The authors also comment on the likelihood of being able to discriminate between the OCS molecule and CO₃ (C_{2v}) which lies in the detection of additional bands associated with these molecules; OCS having additional absorptions around 860 cm⁻¹ (ν₃; 11.6 μm) and 520 cm⁻¹ (ν₂; 19.2 μm), and CO₃ (C_{2v}) which has strong absorption features at 1879 cm⁻¹ (5.3 μm; Fermi resonance) and 973 cm⁻¹ (ν₅; 10.3 μm). In addition, several other absorption features that corresponding to other related CO_x (x = 4–6) species could potentially be identified within this wavelength region (CO₄ (C_{2v}) at 1941 cm⁻¹ (5.2 μm), CO₅ (C₂) at 1912 cm⁻¹ (5.2 μm), and CO₆ (C_s) at 1876 cm⁻¹ (5.3 μm)).^{18–20} The peak positions reported in this work can be directly compared to observations to help aid in the detections of some of these species.

The C : O ratio within interstellar ices is likely to be of significant importance concerning the complexity of species that can be formed within interstellar ices and subsequently released into the gas-phase. The carbon oxides CO_x (x = 4–6) are expected to break-down into simpler molecules such as CO, CO₂, O₂, and O₃ during sublimation of interstellar or solar system ices. In contrast, ices rich in carbon are able to produce linear carbon and carbon oxide chains, many of which are stable upon sublimation of the host ice; several of these species have already been detected in the gas-phase of the interstellar medium, see ref. 16. The role of ice radiation chemistry *versus* gas-phase production of these species may be currently underestimated. As chemical processing is also a source for isotopic exchange between molecules contained within the grain, it is important to also consider these effects as potential sources of isotopic enrichment.

There is a particular relevance of the present set of experiments to the radiolysis-induced processing of apolar ices, which are known to be composed of CO, O₂, N₂, and CO₂. Firstly, as we have already proposed,²⁴ it is likely that the CO₂ observed in these environments is likely a product formed from the processing of these ices. It is highly likely that the other products observed here may also be detectable within these environments. Additionally, it should be noted that when pure CO and O₂ ices are processed, they produce chemical species which are chemically less volatile: *e.g.* CO₂, and O₃, respectively. These chemical species may remain on the outer layers of interstellar ices after the volatile components have been released into the gas-phase, and either processed further or released in subsequent sublimation processes as observed here.

However, from an astronomical point of view, it is important to discuss briefly what information can and cannot be directly applied regarding the reported temperatures of sublimation. One should bear in mind that astronomical timescales are vastly different than those often used in a laboratory. For example, water held at 100 K evaporates on a timescale of a few hundred years⁵⁶ which is a small fraction of time for astronomical models but simply not measurable within the laboratory timeframe. We have chosen to report the temperature range over which we observed sublimation of particular species rather than reporting binding energies. While it is possible to derive an estimation of the binding

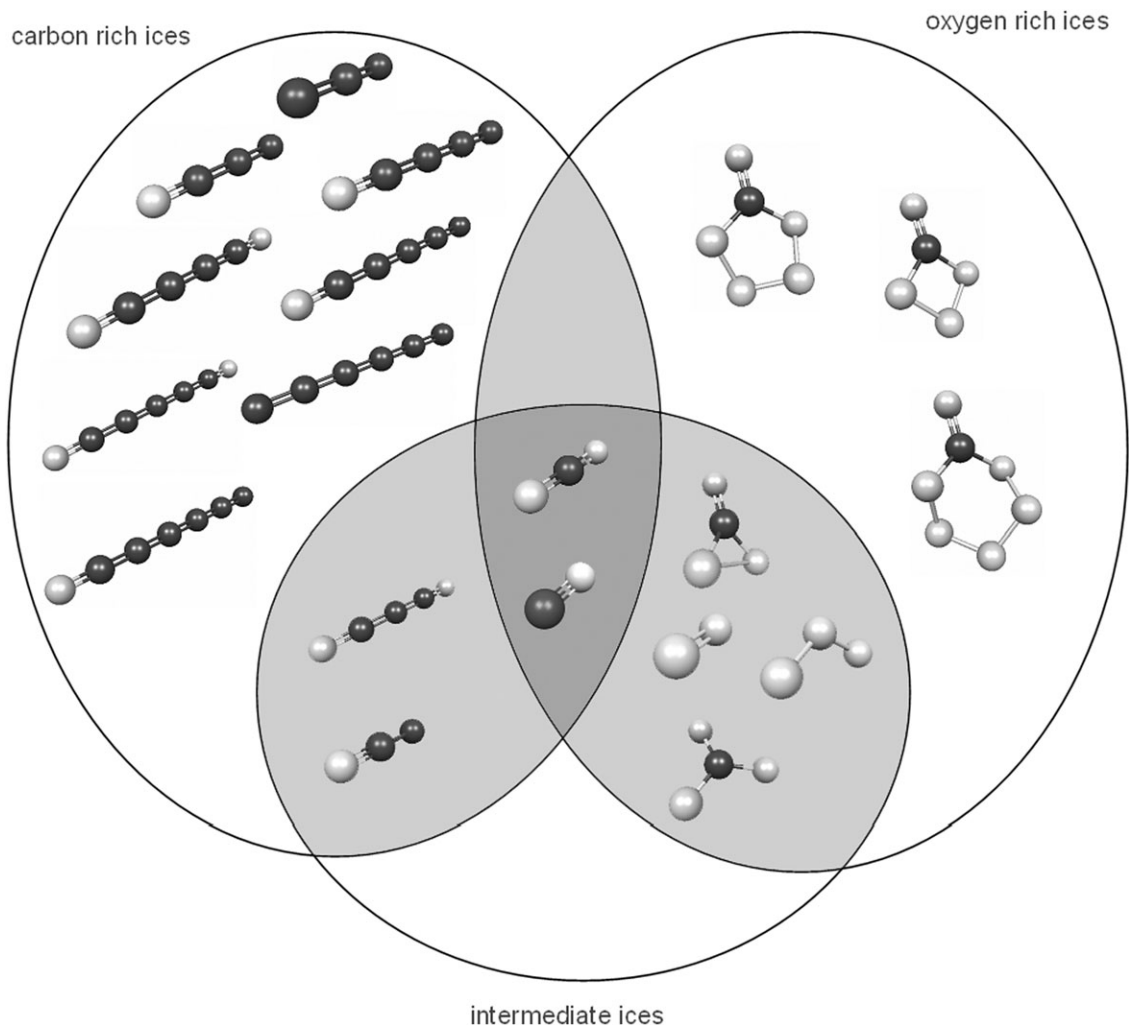


Fig. 5 Summary of products formed within interstellar ices which are either carbon-rich (C : O ratio is 1 or higher), oxygen-rich (C : O is 0.5 or lower), or of intermediate composition. Please see ESI† for a color version of this figure.

energies for the observed species within this work if certain assumptions about our ice morphology are made (as is done in ref. 30), we feel it may be misleading to do so. The precise morphology of a mixed ice is unique depending on the precise deposition conditions which are altered throughout an experiment by the irradiation, as well as thermal processes; the ices likely contain different bonding environments for each species (as well as van der Waals complexes) which will have unique binding energies. The process of sublimation even from a mixed ice that has *not* been subjected to irradiation typically occurs in multiple stages and the binding energies can only be derived from a series of carefully designed experiments,⁵⁷ which can then be incorporated into astronomical models.⁵⁸ Radiolysis-induced processing of mixed ices is likely to complicate the process of sublimation further. The results presented here demonstrate this, but unfortunately only in a qualitative manner.

5. Conclusion

This paper focused on the processing of ice mixtures of varying carbon-to-oxygen ratios from 1 : 1.5 to 1 : 4 in order to determine the underlying principle reactions that are occurring

within interstellar ices and what species may be expected to form as the C : O ratio is altered. The molecular species that are expected to be produced within an interstellar ice can thus be roughly determined whether the ice is classified as: (i) a carbon-rich ice, where the C : O ratio is 1 : 1 or higher, (ii) an oxygen-rich ice, where the C : O ratio is 1 : 2 or lower, and (iii) ices of intermediate composition. Using this classification system, the observable species expected are shown in Fig. 5. Thus, carbon-rich ices are expected to be rich in the same components that are found within the irradiation of pure carbon monoxide ices; linear cumulenenic chains such as carbon chains (C₃ and C₆) together with oxygen-terminated carbon clusters of the series C_nO ($n = 2-7$) and C_nO₂ ($n = 3-5$, and 7). Oxygen-rich ices, on the other hand, are expected to produce species such as those found in pure carbon dioxide irradiated ices: including ozone, and carbon oxide CO_n species (where $n = 3-6$). Ices of intermediate composition are expected to form species which form early during the irradiation of each ice. In our CO : CO₂ experiments, we were able to determine the presence of both species formed during the irradiation of pure carbon monoxide ices (dicarbon monoxide and carbon suboxide) as well as those formed from irradiation of pure carbon dioxide ices (molecular

oxygen, ozone, and two isomers of carbon trioxide). While we were able to monitor trace signals from higher carbon oxides in this experiment (CO₄₋₆), the level of formation of these species here is too low to expect them to be detected in an extraterrestrial environment. The ices studied here are compositionally very similar to apolar ices observed within the interstellar medium.

Further experiments using isotopic mixtures were carried out in order to extract additional mechanistical information. Specific isotopomers of key molecular species were followed quantitatively through infrared spectroscopy during the irradiation procedure, and their profiles were subsequently fit using sequential reaction mechanisms. From this procedure, it was shown that two main reaction types could account for all of the observed kinetics; (i) radiolysis-induced dissociation of the reactants, or (ii) reaction with suprathreshold oxygen atoms (generated during the dissociation). These studies help increase the general understanding of processes that occur during the chemical processing of both interstellar and solar system ices through the interaction of radiation on them.

References

- E. L. Gibb, D. C. B. Whittet, A. C. A. Boogert and A. G. G. M. Tielens, *Astrophys. J. Suppl.*, 2004, **151**, 35.
- M. J. Mumma, M. A. DiSanti, N. Dello Russo, K. Magee-Sauer, E. Gibb and R. Novak, *Adv. Space Res.*, 2003, **31**, 2563.
- J. Crovisier, *Faraday Discuss.*, 1998, **109**, 437.
- T. B. McCord, R. W. Carlson, W. D. Smythe, G. B. Hansen, R. N. Clark, C. A. Hibbitts, F. P. Fanale, J. C. Granahan, M. Segura, D. L. Matson, T. V. Johnson and P. D. Martin, *Science*, 1997, **278**, 271.
- T. B. McCord, G. B. Hansen, R. N. Clark, P. D. Martin, C. A. Hibbitts, F. P. Fanale, J. C. Granahan, M. Segura, D. L. Matson, T. V. Johnson, R. W. Carlson, W. D. Smythe, G. E. Danielson and the NIMS team, *J. Geophys. Res.*, 1998, **103**, 8603.
- B. J. Buratti, D. P. Cruikshank, R. H. Brown, R. N. Clark, J. M. Bauer, R. Jaumann, T. B. McCord, D. P. Simonelli, C. A. Hinnitts, G. B. Hansen, T. C. Owen, K. H. Baines, G. Bellucci, J.-P. Bibring, F. Capaccioni, P. Cerroni, A. Coradini, P. Drossart, V. Formisano, Y. Langevin, D. L. Matson, V. Mennella, R. M. Nelson, P. D. Nicholson, B. Sicardy, C. Sotin, T. L. Roush, K. Soderlund and A. Muradyan, *Astrophys. J.*, 2005, **622**, L149.
- R. N. Clark, R. H. Brown, R. Jaumann, D. P. Cruikshank, R. M. Nelson, J. Buratti, T. B. McCord, J. Lunine, K. H. Baines, G. Bellucci, J.-P. Bibring, F. Capaccioni, P. Cerroni, A. Coradini, V. Formisano, Y. Langevin, D. L. Matson, V. Mennella, P. D. Nicholson, B. Sicardy, C. Sotin, T. M. Hoefen, J. M. Curchin, G. Hansen, K. Hibbitts and K.-D. Matz, *Nature*, 2005, **435**, 66.
- G. Filacchione, F. Capaccioni, T. B. McCord, A. Coradini, P. Cerroni, G. Bellucci, F. Tosi, E. D. Aversa, V. Formisano, R. H. Brown, K. H. Baines, J. P. Bibring, B. J. Buratti, R. N. Clark, M. Combes, D. P. Cruikshank, P. Drossart, R. Jaumann, Y. Langevin, D. L. Matson, V. Mennella, R. M. Nelson, P. D. Nicholson, B. Sicardy, C. Sotin, G. Hansen, K. Hibbitts, M. Showalter and S. Newman, *Icarus*, 2007, **186**, 259.
- W. M. Grundy, L. A. Young and E. F. Young, *Icarus*, 2003, **162**, 223.
- W. M. Grundy, L. A. Young, J. R. Spencer, R. E. Johnson, E. F. Young and M. W. Buie, *Icarus*, 2006, **184**, 543.
- E. Quirico, S. Doute, B. Schmitt, C. de Bergh, D. P. Cruikshank, T. C. Owen, T. R. Geballe and T. L. Roush, *Icarus*, 1999, **139**, 159.
- W. M. Grundy and M. W. Buie, *Icarus*, 2001, **153**, 248.
- T. E. Madey, R. E. Johnson and T. M. Orlando, *Surf. Sci.*, 2002, **500**, 838.
- G. Strazzulla and R. E. Johnson, *Comets in the Post-Halley Era*, Kluwer, Dordrecht, 1991.
- J. F. Cooper, R. E. Johnson, B. H. Mauk, H. B. Garrett and N. Gehrels, *Icarus*, 2001, **149**, 133.
- C. S. Jamieson, A. M. Mebel and R. I. Kaiser, *Astrophys. J. Suppl.*, 2006, **163**, 184.
- C. J. Bennett, C. S. Jamieson, A. M. Mebel and R. I. Kaiser, *Phys. Chem. Chem. Phys.*, 2004, **6**, 735.
- C. S. Jamieson, A. M. Mebel and R. I. Kaiser, *Chem. Phys. Lett.*, 2007, **440**, 105–109.
- C. S. Jamieson, A. M. Mebel and R. I. Kaiser, *Chem. Phys. Lett.*, 2007, **443**, 49–54.
- C. S. Jamieson, A. M. Mebel and R. I. Kaiser, *Chem. Phys. Lett.*, 2008, **450**, 312–317.
- C. S. Jamieson, A. M. Mebel and R. I. Kaiser, *ChemPhysChem*, 2006, **7**, 2508–2513.
- M. L. Delitsky and A. L. Lane, *J. Geophys. Res.*, 1997, **102**, 16385.
- A. C. A. Boogert, M. R. Hogerheijde and G. A. Blake, *Astrophys. J.*, 2002, **568**, 761.
- C. J. Bennett, C. S. Jamieson and R. I. Kaiser, *Astrophys. J. Suppl.*, 2009, **182**, 1–11.
- P. A. Gerakines, W. A. Schutte, J. M. Greenberg and E. F. van Dishoeck, *Astron. Astrophys.*, 1995, **296**, 810.
- R. I. Kaiser, P. Jansen, K. Petersen and K. Roessler, *Rev. Sci. Instrum.*, 1995, **66**, 5226–5231.
- S. A. Sandford, L. J. Allamandola, A. G. G. M. Tielens and G. J. Valero, *Astrophys. J.*, 1988, **329**, 498.
- G. E. Ewing and G. C. Pimentel, *J. Chem. Phys.*, 1961, **35**, 925.
- J. E. Cahill, *J. Chem. Phys.*, 1977, **66**, 4847.
- S. A. Sandford and L. J. Allamandola, *Astrophys. J.*, 1990, **355**, 357.
- I. Wieder and G. B. McCurdy, *Phys. Rev. Lett.*, 1966, **16**, 565.
- N. G. Moll, D. R. Clutter and W. E. Thompson, *J. Chem. Phys.*, 1966, **45**, 4469.
- M. E. Jacox, D. E. Milligan, N. G. Moll and W. E. Thompson, *J. Chem. Phys.*, 1965, **43**, 3734.
- C. J. Bennett and R. I. Kaiser, *Astrophys. J.*, 2005, **635**, 1362.
- L. Brewer and L.-F. Wang, *J. Chem. Phys.*, 1972, **56**, 759.
- L. Schriver-Mazzuoli, A. de Saxcé, C. Lugez, C. Camy-Peyret and A. Schriver, *J. Chem. Phys.*, 1995, **102**, 690.
- B. R. Cairns and G. C. Pimentel, *J. Chem. Phys.*, 1965, **43**, 3432.
- L. H. Jones, S. F. Agnew, B. I. Swanson and S. A. Ekberg, *J. Chem. Phys.*, 1986, **85**, 428.
- J. I. Steinfeld, J. S. Francisco and W. L. Hase, *Chemical Kinetics and Dynamics*, Prentice Hall, Upper Saddle River, 1999.
- J. W. McConkey, C. P. Malone, P. V. Johnson, C. Winstead, V. McKoy and I. Kanik, *Phys. Rep.*, 2008, **466**, 1–103.
- P. A. Gerakines, W. A. Schutte and P. Ehrenfreund, *Astron. Astrophys.*, 1996, **312**, 289.
- P. A. Gerakines and M. H. Moore, *Icarus*, 2001, **154**, 372.
- H. Cottin, M. H. Moore and Y. Bénilan, *Astrophys. J.*, 2003, **590**, 874.
- H. Okabe, *Photochemistry of Small Molecules*, Wiley, New York, 1978.
- P. W. Zetner, I. Kanik and S. Trajmar, *J. Phys. B: At., Mol. Opt. Phys.*, 1998, **31**, 2395–2413.
- C. J. Bennett, C. S. Jamieson and R. I. Kaiser, *Phys. Chem. Chem. Phys.*, 2009, **11**, 4210–4218.
- P. C. Cosby, *J. Chem. Phys.*, 1994, **98**, 7804.
- P. C. Cosby, *J. Chem. Phys.*, 1993, **98**, 7804.
- P. C. Cosby, *J. Chem. Phys.*, 1993, **98**, 9560.
- P. B. Armentrout, *Science*, 1991, **251**, 175–179.
- D. Talbi, G. S. G. S. Chandler and A. L. Rohl, *Chem. Phys.*, 2006, **320**, 214.
- A. M. Mebel, M. Hayashi, V. V. Kislov and S. H. Lin, *J. Phys. Chem. A*, 2004, **108**, 7983–7994.
- J. Elsila, L. J. Allamandola and S. A. Sandford, *Astrophys. J.*, 1997, **479**, 818–838.
- H. P. Larson, D. S. Davis, J. H. Black and U. Fink, *Astrophys. J.*, 1985, **299**, 873.
- T. R. Geballe, F. Baas, J. M. Greenberg and W. Schutte, *Astron. Astrophys.*, 1985, **146**, L6.
- W. Zheng, D. Jewitt and R. I. Kaiser, *J. Phys. Chem. A*, 2009, **113**, 11174.
- M. P. Collings, J. W. Dever, H. J. Fraser, M. R. S. McCoustra and D. A. Williams, *Astrophys. J.*, 2003, **583**, 1058.
- S. Viti, M. P. Collings, J. W. Dever and M. R. S. McCoustra, *Mon. Not. R. Astron. Soc.*, 2004, **354**, 1141.